Hydrogeology Journal (2024) 32:759–784
https://doi.org/10.1007/s10040-024-02766-2

REPORT

Integrating geological, hydrogeological and geophysical data to identify groundwater resources in granitic basement areas (Guéra Massif, Chad)

H. Nouradine[1,2] · C. Schamper[1] · D. Valdes[1] · I. Moussa[2] · D. Ramel[3] · V. Plagnes[1]

Received: 8 May 2023 / Accepted: 7 January 2024 / Published online: 19 February 2024

Abstract

In Chad, hard-rock aquifers are the main source of drinking water for the population located on basement areas. In these basement aquifers, and in particular those of the Guéra region, water drilling failure rates remain high despite research on one- and two-dimensional electrical resistivity techniques and lineaments as a means to improve access to the resource, mainly because these techniques are only used on an observational and structural basis to locate fractures. This study combines electrical resistivity tomography (ERT) with geology, hydrogeology and geomorphology, in order to characterise the structure and geometry of the aquifer system, assess borehole productivity and determine the factors controlling it. After validating the large dataset and its representativeness, 315 high- and low-yield wells, of which 41 have complete geophysical datasets, were selected. This large dataset allows a multi-parameter approach to (1) better characterise each facies according to its electrical resistivity and (2) clearly identify the main formations constituting the local conceptual hydrogeological model. The most suitable areas for productive boreholes are characterised by the presence of an overburden of <20 m depth, well-developed weathered and fractured horizons of granites and biotite granites (preferably) containing little or no clay, and a nearby drainage network. The most substantial flow rates are found in the first 30 m of the fissured horizon, below the base of the alterites. The experience gained from the present study will guide future analysis of ERT sections in order to reduce the probability of drilling dry wells.

Keywords Hard-rock aquifers · Electrical resistivity tomography · Geology · Well productivity · CHAD

✉ H. Nouradine
nouradineh@yahoo.fr

C. Schamper
cyril.schamper@sorbonne-universite.fr

D. Valdes
daniele.valdes_lao@sorbonne-universite.fr

I. Moussa
imoussa2010@gmail.com

D. Ramel
david.ramel@anteagroup.fr

V. Plagnes
valerie.plagnes@sorbonne-universite.fr

1 Sorbonne Université, UMR SU CNRS EPHE 7619 METIS, Paris, France

2 University of N'Djamena, Department of Geology, N'Djamena, Chad

3 Antea Group, Orléans, France

Introduction

Groundwater is a major source of the world's drinking water (Howard et al. 2006). The current context of global climate change is of concern for the development of groundwater resources, as it is marked by an increase in temperature that could lead to changes in evapotranspiration rates in many regions of the world (IPCC 2014; Sagna et al. 2015; Lemaitre-Basset et al. 2022). This could lead to modification of groundwater recharge (Taylor et al. 2013).

This is especially true in sub-Saharan Africa, where there is often no surface water for much of the year. Furthermore, demographic growth in this region, which is the highest in the world (~2.7%/year compared to 0.3–1.8% elsewhere; Leridon 2015), will lead to an explosion in demand for water in coming years. This evolution is accompanied by economic and industrial development with consequences for groundwater resources, both in terms of quality and quantity (MacDonald et al. 2012; Gaye and Tindimugaya

2019). These groundwater issues will be all the more important in areas with basement rocks (plutonic and metamorphic), known for their heterogeneity and the difficulty in supporting productive wells. These rocks cover ~40% of the African continent (Taylor and Howard 2000; MacDonald et al. 2012) and are exposed to deep weathering processes (Lachassagne et al. 2021). The exploitation of groundwater resources in these aquifers remains a major challenge for hydrogeologists in the sub-region. In Benin, Burkina Faso and Côte d'Ivoire, the failure rate of wells located in basement areas is between 30 and 40% (Courtois et al. 2010; Vouillamoz et al. 2014; Alle et al. 2018). In these environments, the most productive zones have been established as the alterite layers which are the thickest and comprise the least clay, alongside the well-developed fissured/fractured stratiform horizons of the first few meters. These zones (or aquifer layers) provide storage and transmissive roles, respectively (Vouillamoz et al. 2015; Alle et al. 2018; Lachassagne et al. 2021). The productivity of the wells setup in hard rocks is generally modest, from a few hundred to a few thousand litres per hour (Courtois et al. 2010; Maurice et al. 2019). Electrical resistivity tomography has proved useful in characterising the different compartments of hard-rock aquifers through fairly accurate imaging of the weathered profile—see, for example, Soro et al. (2017), Alle et al. (2018), Belle et al. (2019), Nesny et al. (2019), Foppen et al. (2020), Briški et al. (2020), Leborgne et al. (2021), Maurya et al. (2021), Ouedraogo et al. (2022), Olivier et al. (2022)—but each of these studies concerns only a limited number of sites and data.

Like most countries in sub-Saharan Africa, Chad mainly uses not only groundwater but also surface water to meet the drinking water needs of its population and to ensure the development of socio-economic activities. However, regions characterised by a plutonic and metamorphic rock basement, such as the Guéra region, face considerable problems in accessing drinking water. Indeed, the needs of the rural population and its main activities are generally met by surface water during the rainy season. During the dry season, villagers use surface water (alluvium, alterites) through traditional wells. These aquifers are highly dependent on rainfall (Schneider 2001). In most cases, they are exhausted before the rain returns. To overcome these problems, deep hard-rock aquifers are an interesting alternative because, potentially, they constitute a longer-term and better-quality water resource (Lachassagne et al. 2021). Despite the progress made, the percentage of negative wells (development flow rate of less than 0.5 m^3/h), or even dry wells, remains very high, at ~57% in the area considered here (10th FED 2016). Wells with a development flow rate of 0.5 m^3/h or more are considered high-yield (from this flow rate onwards, wells can be equipped and operated by a human-powered pump within the framework of hydraulic projects). This high percentage of failure is linked, on one hand, to the limits of the prospective operational methods generally applied and, on the other, to insufficient knowledge of local hydrogeology. Initially, the PHPTC1/AFD (2008) and PHPTC2/AFD (2013) programmes set up wells by systematically conducting electrical profiling and one-dimensional (1D) sounding. During a second phase, the 9th FED (2011) and 10th FED (2016) programmes applied both electromagnetic profiling (EM34) and electrical resistivity tomography (ERT, 2D) on lineaments identified through aerial photography and satellite imaging. The latter method proved better suited, but the data were used only to identify structures qualitatively, locating individual fractures without taking into account their environment: geometry, lithology, topography, hydrography, lineament density, connectivity with other structures, etc.

In truth, hard-rock aquifers in Chad have been subject to little in-depth geophysical work. Among the studies carried out, there is that of Abderamane et al. (2018) in the Guéra region, based on lineaments, electrical profiling and sounding (1D), and those of Oursingbé et al. (2012) in Lac-iro (Lake Iro) region, and Dinard et al. (2021) in Ouaddaï region, but based on the electrical resistivity tomography (2D) of limited data.

The present study aims to characterise the hydrogeology and the properties of the main hard-rock aquifer formations—thickness, nature, electrical resistivity ranges, flow rates assessment—with the aim of determining the factors that control productivity in order to increase the probability of successfully installing wells. The study is based on a large and multidisciplinary dataset: 315 high- and low-yield wells with complete and validated technical data; for 41 of them, reinterpreted ERT geophysical data have been added. This is the first study cross-referencing data on well productivity with that from electrical resistivity tomography, geology and geomorphology.

Hard-rock aquifers: conceptual models and hydrogeology

For several years now, studies on basement aquifers in Africa and around the world have led to the development of several conceptual models adapted to different basement zones. Historically, many authors have considered that productivity of hard-rock aquifers is controlled by fractures resulting from tectonic phenomena or decompressions (Lachassagne et al. 2001; Sander 2007; Kamagaté et al. 2007; Kouamé et al. 2010). More recently, other research has demonstrated that mineral weathering is in fact the main driver of fracture development within these hard rocks, making them suitable as aquifers and allowing the flow of significant groundwater (Dewandel et al. 2006; Lachassagne et al. 2011, 2014; Worthington et al. 2016).

A typical weathered profile comprises layers that have distinct and specific hydrodynamic properties. These layers form a composite aquifer described from top to bottom as follows (Wyns et al. 2004; Dewandel et al. 2006, 2011; Lachassagne et al. 2011, 2014):

1. A laterite or bauxite layer, which may be absent. Where it is preserved from erosion and recharged by heavy rains, it may give rise to small, hilltop pools which dry up during the dry season.
2. Saprolite (also called alterites), formed from a mixture of weathering by-products (sand, clay, hydroxides or oxides and residual minerals (quartz). Generally, in the lower part, isalterites can be found and the structure of the parent rock is generally preserved (porosity substitutes the evacuated material). In contrast, in the upper part, the structure of the rock has disappeared, and the rock contains alloterites. At the top of the saprolite, mottled clay, ~1 m thick, forms a transitional horizon with the laterite/bauxite layer. In coarse-grained rocks (granitoids, gabbros), the lower part of the saprolite takes on a laminated appearance (laminated horizon) which results from the spacing between joints of the fractured horizon narrowing down to millimetres. This part of the weathered profile is not very permeable but relatively porous and can hold water (Dewandel et al. 2006). This is often the storage part of the aquifer.
3. The fractured horizon is characterized by dense fracturing in the first few meters which decreases with depth. Its thickness also reaches several tens of meters; it is generally double that of the saprolite (Dewandel et al. 2017; Wyns 2020). Only some of the minerals in the rock are weathered, so the rock remains hard as a whole and permeable. This part of the weathering profile allows the groundwater to flow (Wyns et al. 2004; Dewandel et al. 2006).
4. Unweathered rock is not permeable, except sometimes in specific locations, where certain discontinuities (old tectonic fractures, veins, dykes, contact zones between different lithologies, etc.) have enabled weathering to occur at greater depths (Maréchal et al. 2004; Bouchot et al. 2011).

This report uses the following terminology (based on the conceptual model of Wyns et al. 2004 as presented in Fig. 1): *overburden* (O), assigned to the laterite or bauxite layer or other sedimentary deposits; *weathered horizon* (WH), assigned to the saprolite (the upper layer of unconsolidated and consolidated weathered rocks); *fractured horizon* (FH); and *unweathered hard rock* (UW).

This conceptual model has led to several operational hydrogeological applications. These include: mapping of the main hard-rock aquifers from topographic maps, digital elevation models (DEMs), geological field observations, well data (Lachassagne et al. 2001; Wyns et al. 2004; Dewandel et al. 2006; Courtois et al. 2010); statistical analysis of parameters influencing productivity (Dibi et al. 2004; Koudou et al. 2013; Maxime et al. 2014; Odile et al. 2015; Ewodo Mboudou et al. 2018); machine learning for the identification of suitable areas (Gómez-Escalonilla et al. 2021, 2022); and geophysics, in this case, electrical resistivity tomography to characterise the structure and geometry

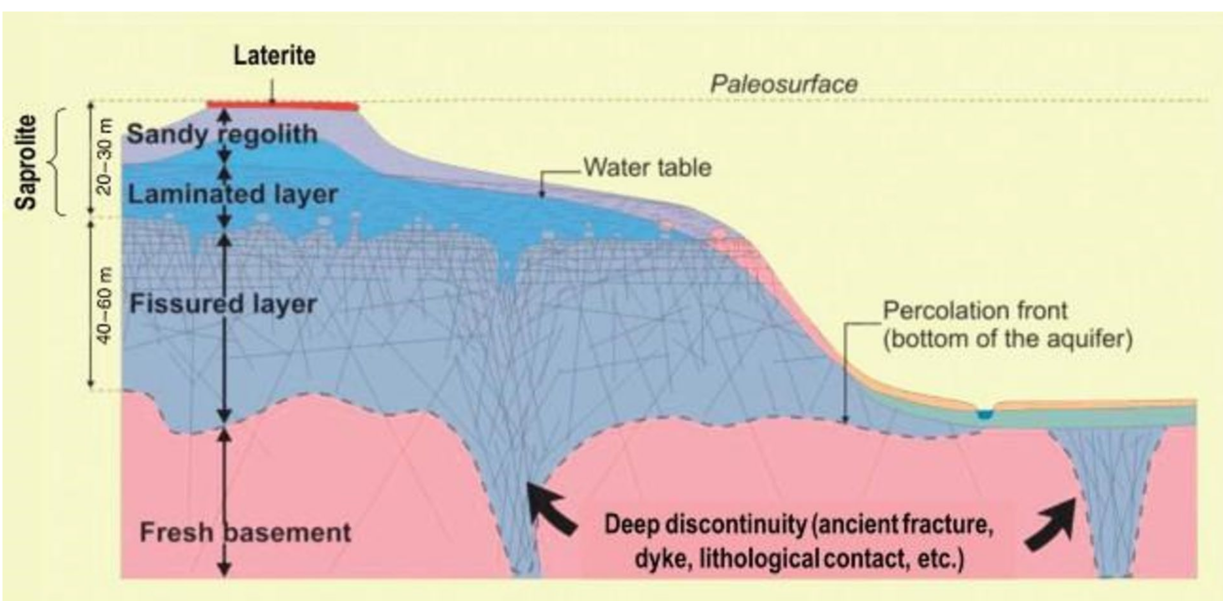

Fig. 1 Conceptual model of weathering in a hard rock aquifer (Wyns et al. 2004)

of the weathered profiles (Soro et al. 2017; Alle et al. 2018; Belle et al. 2019; Ouedraogo et al. 2022).

Study area

The region of Guéra, located in central Chad and extending between 10° and 14° north and between 18° and 20° east (Fig. 2), covers an area of 23,262 km^2 with a population of ~550,000 inhabitants across 700 villages, according to the population and housing general census (INSEED 2009). Administratively, it is subdivided into four departments: Abtouyour, Guéra, Bahr Signakha and Mangalmé. The area studied covers the departments of Abtouyour (Bitkine) and Guéra (Mongo), selected as pilot sites because of the low water supply rate (13 and 22% respectively) and the availability of quality geological, geophysical and hydrogeological data from international programmes (PHPTC1/AFD 2008; 9th FED 2011; PHPTC2/AFD 2013) (Fig. 2).

The region has a Sahelo-Sudanese type climate (430–867 mm/year). In all, 60–70% of the rain falls during July and August, often with high intensity. The low

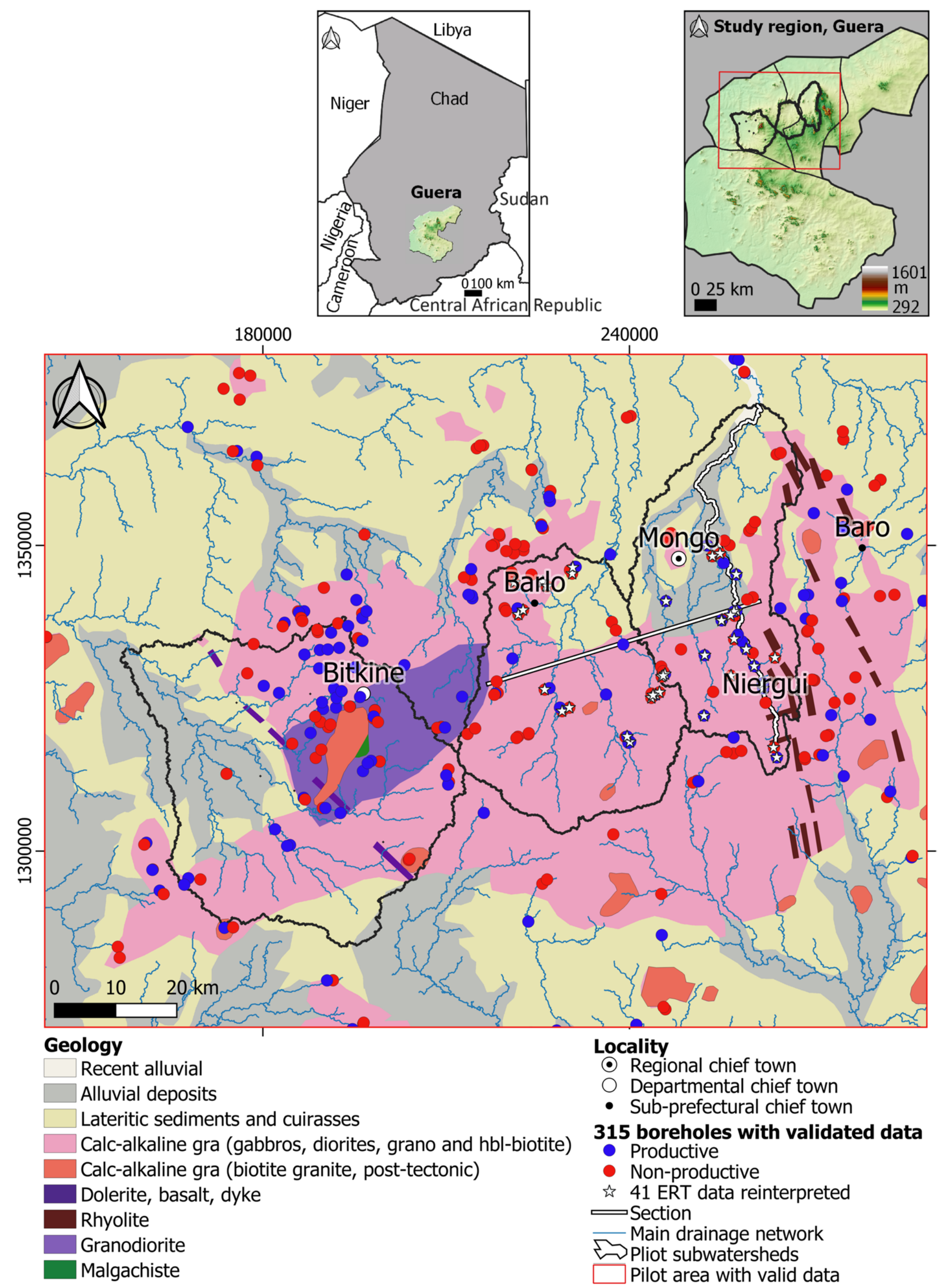

Fig. 2 Location and geological context of the study area including the selected sites—productive boreholes (Qd ≥ 0.5 m^3/h) and non-productive boreholes (Qd < 0.5 m^3/h)

vegetation cover and the relief mean that runoff predominates over infiltration on both plateaus and slopes.

Geologically, the region is part of the Guéra Massif, made up of an orographic unit comprising three main mountain ranges—Aboutelfan, Kengas and Melfi—as well as numerous small secondary mountain ranges and inselbergs separated by sandy open spaces. The Guéra Massif culminates at 1,613 m at the peak of Guéra, while the mean elevation of the surrounding plain varies between 400 and 500 m. This Precambrian massif is essentially made up of magmatic formations, of which 90% are granitoids, and some metamorphic rocks. These Precambrian rocks are locally covered by recent formations, Tertiary to Quaternary, including laterite layers, associated with the "Continental Terminal", and fluvio-lacustrine (comprising clay; called pediments) or fluvial alluvia, the latter predominantly sandy and covering recent to present-day water courses (Schneider 1989; Schneider and Wolf 1992; Kusnir 1995).

In addition to granitoids (diorites, granodiorites, granites, charnockites), the magmatic rocks include rare gabbro, found east of Bitkine (Kusnir 1995). The chemical differentiation from the most basic to the most felsic is consistent with the relative age of formation, from oldest to youngest (Isseini et al. 2013). The weathering of granite leads to sandy by-products, which accumulate in valleys crossed by rivers. Conversely, diorites and gabbro produce a characteristic black clay through weathering.

Isseini et al. (2013) distinguished four groups of rocks on the surroundings of Mongo, based on the relative timing of their emplacement, affected by four phases of deformation: (1) the first group, consisting of gabbro, formed prior to the crystallisation of (2) diorites, granodiorites, and hornblende-biotite granites (granites I), followed by (3) the formation of two-mica granites (granites II), intruded by (4) the biotite granites (granites III). The first two groups of rocks are affected by the D1 and D2 deformation phases. They are pretectonic with respect to the third deformation phase D3, responsible for the development of NNE–SSW to ENE–WSW oriented shear zones. Whereas the two-mica granites are syntectonic and the biotite granites are posttectonic. Finally, the last deformation phase D4 is ubiquitous and responsible for the formation of brittle structures in which late dolerite intrusions occur.

The hydrogeology in this area is characterised by discontinuous and localised hard-rock aquifers. There are shallow, porous aquifers (in alluvial or alterite deposits) that overlie discontinuous aquifers in certain areas, within fractures and fissures of the crystalline hard rock. These aquifers have features in common with the conceptual models described by Wyns et al. (2004) and Lachassagne et al. (2014).

Materials and methods

Available raw data and data validation

The data used in this study come from the Drinking Water Access Programme and Support for Sector-Based Policies, piloted by the ministry in charge of water in Chad (9th FED 2011). The database contains complete hydrogeological and geophysical information from 798 wells, 700 EM34 profiles and 592 ERT surveys at the regional level. For productive boreholes, equipment has been installed (screen and filter bed), and nonproductive boreholes have not been equipped. The database contains the geographical coordinates of the wells, the state of the infrastructure, the position of the well screens (top and bottom), the top of the gravel pack, the drilling flow rate, the development flow rate and the pumping rate, piezometric levels (drawdown and rest), the depth of the unweathered bedrock, the total depth of the well, the borehole logs, as well as the electrical profiles and ERT together with their geographical coordinates. However, these data contain uncertainties. The geographical position of each well was checked and corrected where needed. After validation, 315 sites (140 of which have a development flow rate of at least 0.5 m^3/h) covering the departments of Bitkine and Mongo were retained. Of these 315 sites, only the ERT data from 41 sites located in the Mongo and Barlo watersheds were further selected (Fig. 2). These two watersheds share a common drainage network towards the north and were selected because of their low well success rate and the amount of data available, and because they are representative of the geology and geomorphology of the targeted region.

The hydrogeological data (technical data on the wells and on pumping) were subject to: (1) data entry and organisation, (2) data quality validation by cross-referencing parameters and (3) calculations/deductions based on different parameters, e.g., estimating the roof and base of each formation. Geophysical data were subject to (1) quality validation and (2) reprocessing and reinterpretation.

Geological data and productivity

Lithology

The physical parameters of the wells, namely overburden thickness (TO), weathered horizon thickness (TWH), fissured horizon thickness (TFH), thickness above the hardrock (TAHR) and total depth, were extracted from the well logs and analysed. As the boundary between the weathered and fractured horizons can be difficult to distinguish, and to fully quantify the weathered formations, the parameters

(1) sum of the weathered and fissured horizons thicknesses [T(WH+FH)] and (2) sum of the overburden and the weathered horizon thicknesses [T(O+WH)] were added. Other new parameters were also included, such as depth of the roof and of the base of each different formation. Two groups were distinguished according to the nature of the lithology: group GRA, which includes the wells located in granite and biotite granite, and group DIO, representing the wells located in diorite, granodiorite and dolerite.

Productivity

This study includes two productivity measures: total well productivity and horizon productivity.

Well productivity The database contains three different flow rates: (1) the end-of-drilling flow rate (Qf), which corresponds to the volume flow rate from an airlift pump and measured following the water inflows in the various horizons up to the end of drilling (the flow rate presented here is the total end-of-drilling flow rate); (2) the development flow rate (Qd), obtained after development, blowing and equipping, also measured with the same compressor used for the end-of-drilling flow rate, and (3) the step pumping flow rate (Qp), corresponding to the flow rate measured after a three-step pumping test, 2 h/step, using a submersible pump. Figure 3 shows a comparison between these three flow rates.

The flows Qd and Qf (Fig. 3a) have a good overall correlation, with an acceptable correlation coefficient of $R^2 = 0.62$. In most cases, Qd is equivalent to Qf, showing that the boreholes have been properly equipped. However, along the y-axis, some boreholes show a very high Qf compared to Qd. This situation is generally explained by poorly dimensioned equipment or equipment that is not adapted to the productivity levels of the aquifer. Moreover, Qd is more representative of actual borehole productivity than Qf if a productive horizon (alterites) was isolated during drilling. Finally, Qf is not always reliably indicated on the drill logs. For all these reasons, the rest of the study is based on Qd, the values of which are close to Qf, show the quality of the drilling equipment and are representative of the fissured horizon's rate of production.

Flow rates Qd and Qp (Fig. 3b) also show an acceptable correlation ($R^2 = 0.66$); however, it should be noted that Qp is often higher than Qd. Qp is directly dependent on the capacity of the pumps used and is therefore not very representative of aquifer productivity. The development flow rate (Qd) is therefore retained for the remainder of the analysis as it better reflects the conditions of the well.

Productivity of each horizon The flow rates for each horizon correspond to the volumetric flow rates measured during drilling operations in the water inflow zones of the various horizons crossed, using an air-lift pumping system. This gave the following parameters—overburden flow rate (QO), weathered horizon flow rate (QWH) and fractured horizon flow rate (QFH)—which were analysed with the rest of the dataset.

Geophysical data acquisition and reinterpretation

Geophysical data acquisition was carried out by preliminary remote sensing as described in the 9th FED report (2011). This consisted of determining the supposed lineaments of suitable sites, based on the reinterpretation of radar images

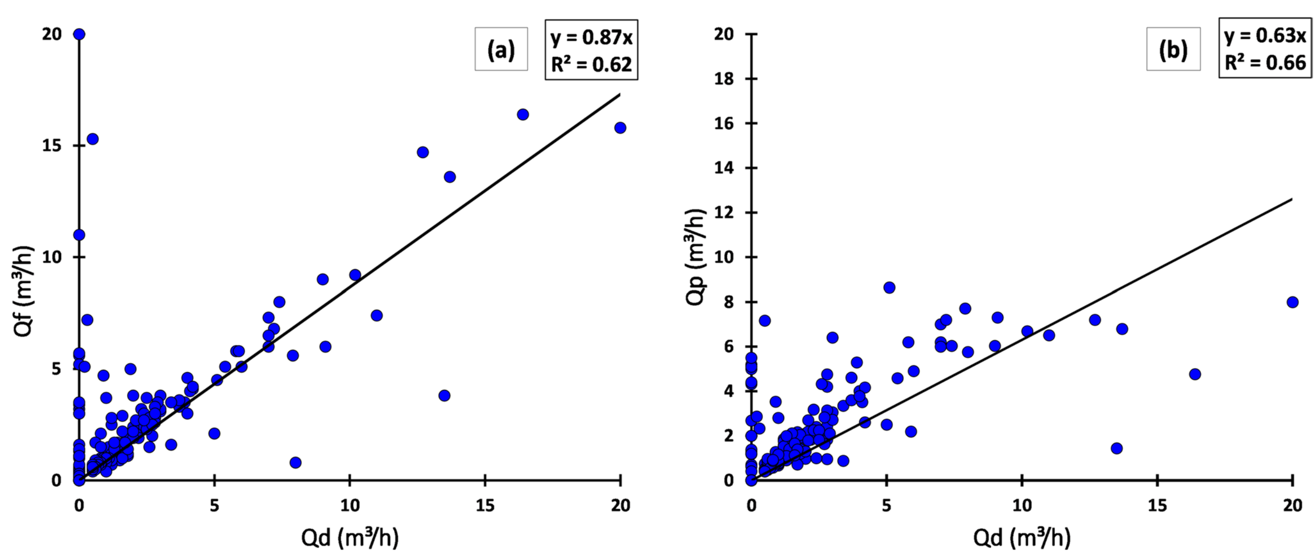

Fig. 3 Relationships between **a** Qd and Qf and **b** Qd and Qp

from the Japanese Earth Resources Satellite (JERS), operating in the L-band (23.5 cm) in HH polarisation, with a spatial resolution of 18 m. The aim was to identify up to three sites (or more if possible) close to villages, preferentially within a radius of 3–4 km around each village, in order to limit the distance beneficiaries would have to travel for water. These suitable sites are called "FB points".

The implementation methodology was as follows:

- A 100-m long EM34 profile centred on a "FB point" was carried out to (in)validate the lineament detected from the reinterpreted radar image. Measurements were taken along an axis perpendicular to the anomaly in question and at regular intervals of 10 m, tightened to 5 m over 20 m before and 20 m after the "FB point". The diagrams drawn up from the measurements provide information on the existence and position of the anomalies, their dip and the average conductivity of the terrain. A comparison of the horizontal and vertical measurements allows an estimate of overburden thickness and the depth at which the anomaly was detected.
- Setup of an ERT survey—SYSCAL R1PLUS SWITCH 48 (200 W, 2500 mA, 600 V)—in a Wenner-Schlumberger array, along a 235 m profile (48 electrodes spaced 5 m apart).
- Setup of an ERT survey in a pole-dipole forward array along a 235 m profile (48 electrodes spaced 5 m apart).
- Setup of an ERT survey in a pole-dipole reverse array along a 235 m profile (48 electrodes spaced at 5 m).
- Inversion of the acquired data and geophysical interpretation.
- Drilling of boreholes.

The inversion was carried out through the RES2DINV (Loke and Barker 1996) computer program after combining the data from the forward and reverse pole-dipole ERT surveys. After performing a few "smooth" inversions in L2 norm favouring gradual changes in resistivity, the terrain was found to be too contrasting. Therefore, "robust" or "blocky" inversions in the L1 norm were applied, making it possible to construct models with more pronounced transitions (Loke et al. 2003). Thus, blocky inversions facilitate tracing the boundary between the weathered profile and the unweathered hard rock (Belle et al. 2019).

The 41 ERT surveys along the two watersheds of Mongo and Barlo were reinterpreted. The inverted electrical resistivities were associated to the lithology and then interpolated onto a regular grid, every 20 cm, perpendicular to the boreholes, enabling the identification of the main geological features: the overburden, the weathered horizon, the fissured horizon and the basement, as well as the range of electrical resistivity (ρO, ρWH, ρFH and ρUR). A morphometric analysis was also conducted describing the geophysical models and the lithology. Data processing involved the use of the following computer programs: ProsysII, RES2DINV, Surfer, MATLAB and GIS.

Development of the geoelectrical conceptual model

The structure and geometry of the weathering profile is based mainly on the mapping of the main formations (from the data of the borehole logs) and the interpretation of electrical resistivity ranges (after the inversion results of the ERT data). First, thickness data for each horizon from the 315 points in the database were interpolated using kriging. This method resolves data estimation problems by considering the spatial variations of the variables processed (Matheron 1966; Ruelle et al. 1986). Second, from the thickness data and the digital elevation model (DEM), the elevation of each horizon (base and/or roof) was calculated. To avoid interpolating the thickness of the overburden and of the weathered horizon in areas where the basement rock outcrops, 468 artificial points were created in these areas and a value of zero was given to overburden (TO) and weathered horizon (TWH) thicknesses, representing the reality in the field. The results of this method were then coupled with those from the geophysical survey to build a geoelectrical conceptual model of hard-rock aquifers in the region.

Statistical analysis of geological, hydrogeological and geophysical parameters

Validation and processing of the data led to a new database of 315 sites with 62 parameters of which 15 were selected for this study (Table 1). Statistical analyses were carried out to assess borehole productivity and understand the main criteria controlling it.

Elementary statistics represented by box plots were carried out on the 15 parameters selected in order to highlight the standard deviation (SD), coefficient of variation, and minimum, maximum, mean and median values for each parameter. These statistics were also used to analyse the parameters according to the different geophysical models.

A comparative analysis of development flow rates (Qd) in relation to total depth (TD) and the thicknesses of different formations (TO, TWH and TFH) was also carried out to determine the most productive horizons and indicate the optimum depths not to be exceeded when drilling.

Multivariate analysis, i.e., a standardised principal component analysis (PCA) was conducted on the 15 parameters selected. PCA allows the simultaneous study and synthesis of the relationships between several variables (Dibi et al. 2004; Valdes 2005), highlighting associations that could be influenced by more than one factor.

Hydrogeology Journal (2024) 32:759–784

Table 1 Parameters used in this study and their units of measure

Parameter (units)	Description
Z (m)	Elevation
Qd (m^3/h)	Development flow rate
TO (m)	Overburden thickness
TWH (m)	Weathered horizon thickness
QWH (m^3/h)	Weathered horizon flow rate
TFH (m)	Fractured horizon thickness
QFH (m^3/h)	Fractured horizon flow rate
T(WH+FH) (m)	Total thickness of weathered and fractured horizon
TCO (m)	Clay overburden thickness
T(O+WH) (m)	Total thickness of overburden and weathered horizon
TAHR (m)	Thickness above hard rock
TD (m)	Total depth
ρO (Ωm)	Resistivity of the overburden
ρWH (Ωm)	Resistivity of the weathered horizon
ρFH (Ωm)	Resistivity of the fractured horizon

Two normalised principal component analyses (NPCAs) were carried out. The first one, at the regional scale (315 sites), analysed well productivity against 12 geological parameters (Z, Qd, TO, TWH, QWH, TFH and QFH as active variables, and TCO, T(WH+FH), T(O+WH), TAHR and TD as supplementary variables) for 315 individual sites, of which 29 are considered as supplementary sites as they do not present all the variables. The second NPCA was run at the scale of the two watershed areas and included the geophysical variables that resulted from the reprocessing carried out for the present study (resistivities estimated for the overburden ρO, and the weathered ρWH and fractured ρFH horizons). This second NPCA was carried out on 15 variables (including Z, Qd, TO, TWH, QWH, TFH and QFH as active variables, and TCO, T(WH+FH), T(O+WH), TAHR, TD, ρO, ρWH and ρFH as supplementary variables) for 41 individual sites, seven of which counted as supplementary sites according to the same criteria cited above for the first NPCA.

There are different reasons for including additional variables. Firstly, weathered and fractured horizons cannot be distinguished with certainty in the geological logs (and also through resistivity values), which is why variable T(WH+FH) was calculated. It sums up the thickness of these two horizons. Secondly, the thickness of the clay overburden (TCO) is already included in the overburden thickness. The sum of the overburden and the weathered horizon thicknesses (T(O+WH)), which also corresponds to the total thickness of unconsolidated formations (TAHR), is included as a variable in order to minimise the possibility of excluding the weathered layer as a whole from the analysis. Furthermore, the total depth of drilling (TD) does not seem to be a relevant parameter given that the depth depends on the well yield test, the deepest boreholes often being those that do not have a high yield. Finally, electrical resistivities for the different formations are only available for 41 sites. Considering them as additional variables allows a comparison between the two NPCAs, the first on 315 sites and the second on 41.

Results and interpretation

Descriptive statistics of the main parameters retained for this study

Figure 4 presents statistics for all 315 sites and the subset of 41 watershed sites (two watersheds) for the parameters studied for each of the different rocky formations and wells: thickness and depths of the different horizons, the flow rates and the resistivities of the different horizons. The mean values calculated for all 315 and for the subset of 41 sites are fairly similar, indicating that the two watershed areas are representative of all the points located in the region.

Well productivity

In the Guéra region, well development flow rates (Qd) vary from 0 to 20 m^3/h with a mean of 1 m^3/h and a SD of 2.58. The histogram on the flow rates for the 315 regional sites (Fig. 5a) shows that 58% of the wells have low to null flow rates (Qd < 0.5 m^3/h), 32% have medium flow rates (0.5 < Qd < 3.5 m^3/h) and only 10% have high flow rates (Qd ≥ 3.5 m^3/h). Consequently, most wells in the region fall into the low flow rate category. The distribution of flow rates for the subset of 41 sites—where the

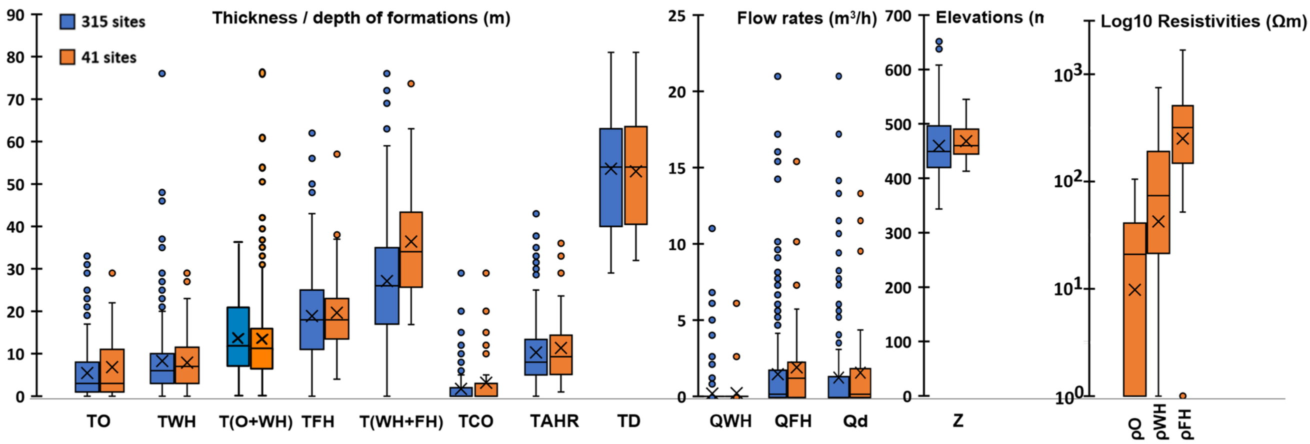

Fig. 4 Statistics for the parameters calculated on all 315 sites (blue) and the subset of 41 sites (orange). Crosses correspond to arithmetic means and dots to the outliers which exceed the whiskers of the box plots (min = Q1 – 1.5 × (Q3 – Q1) and max = Q1 – 1.5 × (Q3 – Q1) with Q1 the 25th percentile and Q3 the 75th percentile)

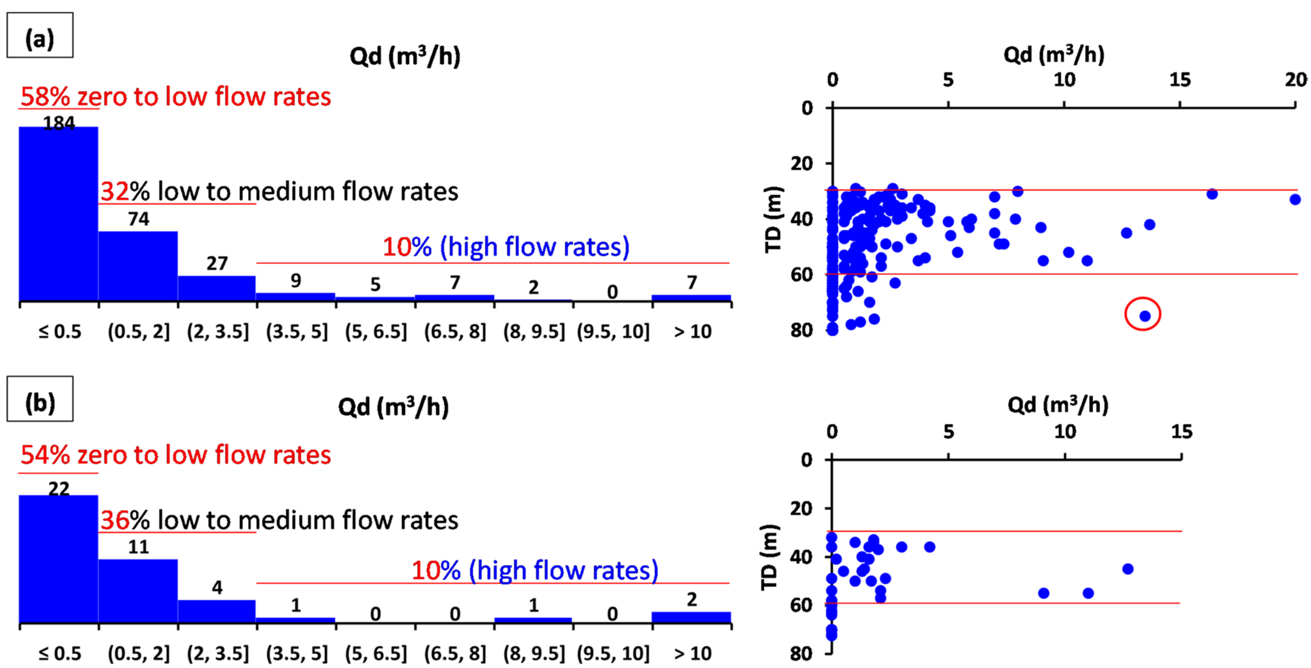

Fig. 5 Development flow rate histograms and relationship between development flow rates and feature depths for **a** 315 sites and **b** 41 sites

geophysical data were reinterpreted (Fig. 5b)—is comparable to that of the 315 regional sites. A close look at the graph on flow rates and depths (Fig. 5a,b) reveals that the highest flow rates (Qd ≥ 5 m^3 /h) are observed at a depth between 30 and 58 m, regardless of the dataset analysed (315 or 41). For depths greater than 58 m, the rates tend to decrease, except for one point located at 75 m. This particular well possibly intersects a deep tectonic fracture facilitating the flow of water. The data representing the subset of 41 sites are therefore consistent with those observed for the larger dataset (315 sites) and the remainder of the study can focus solely on the wells and geophysical profiles of the two watershed areas of Mongo and Barlo (41 sites).

Geological characterisation of formations

Role of the different horizons on productivity

A thickness map for overburden, weathered horizon and fractured horizon thicknesses was drawn using the data from the 315 sites studied. Development flow rates (Qd) were plotted onto this map (Fig. 6) to illustrate the role of each horizon on the productivity of the wells.

The overburden map for the studied area (Fig. 6a) indicates that overburden thickness varies from 0 to 33 m, with a mean of 5 m. Geological logs indicate that the overburden comprises more or less sandy compact clay or laterites with lateritic clay, clay, sandy clay, clayey sand and sand. The map shows that the least thick overburden is in the foothills and the thickest in the valleys. The most productive wells are located in places where the overburden thickness varies between 2 to 20 m.

The weathered horizon map (Fig. 6b) shows that thickness ranges from 0 to 76 m. Figure 6b shows that the highest flow rates correspond mostly to a weathered horizon

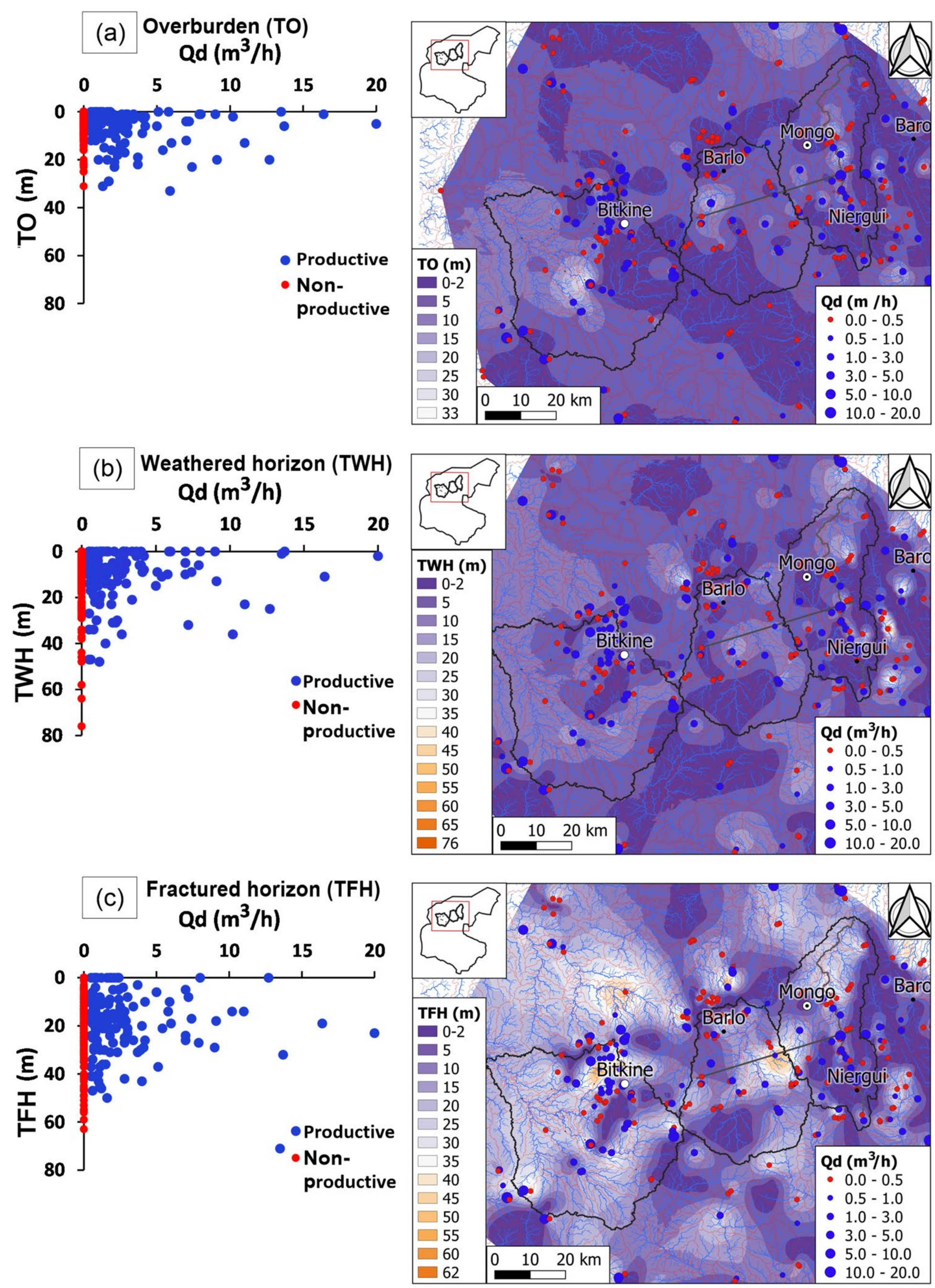

Fig. 6 Characteristics of the three studied horizons: **a** Overburden, **b** Weathered horizon, and **c** Fractured horizon. These are thickness maps from 315 sites and relationship between thickness and development flow rates. Maps were generated using kriging interpolation

thickness of less than 35 m, whereas over 35 m, flow rates tend to decrease.

The fractured horizon map (Fig. 6c) shows a heterogeneous thickness, ranging from 0 to 62 m. The highest flow rates come from the top 30 m of this horizon. This section corresponds to a crack or fracture high-density zone, as described in the model by Lachassagne et al. (2001), Wyns et al. (2004) and Dewandel et al. (2006). Once past the first 30 m, the frequency of fissures decreases and consequently, so do flow rates.

Role of the lithology on productivity

To study the role of lithology on well productivity, two groups were distinguished based on the lithological data from the wells: wells located in granites and biotite granites (GRA group) and those located in diorites, granodiorites and gabbros (DIO group). Figure 7 shows the distribution of productivity according to these two groups. Wells located in granite (GRA group) are significantly more productive than wells from the DIO group. Seventy-five percent of wells from the GRA group have a Qd > 0.5 m^3/h, representing 14 wells in the Mongo basin, ten of which are high-yield, and ten wells in the Barlo watershed, five of which are high-yield. Conversely, only 25% of DIO group wells have a Qd > 0.5 m^3/h, representing ten wells in the Mongo basin, five of which are high-yield, and seven in the Barlo watershed, all of which are classed as low-yield. The highest flow rates (>3 m^3/h) are found exclusively in wells located in granites. This disparity could be due to the weathering processes that affect differently these two lithologies. The granite appears to have more extensive weathering than the other group, possibly favouring aquifer storage and well productivity. Lithology appears therefore of considerable interest for future exploration.

Hydro-geophysical characteristics of the rocky formations

The 41 site surveys show electrical resistivities between 10 and 13,000 Ωm with normalized absolute error (L1 norm or robust inversion considered to explain the data) varying between 2.3 and 15.5%.

Resistivity ranges of the different formations

To determine the resistivity ranges of the different formations, the 41 profiles were analysed (see section 'Materials and methods'). The histograms in Fig. 8 represent the results. The two watersheds have one main difference: the absence of overburden in the Barlo area; nonetheless, the different horizons have the same resistivity ranges in both areas. This approach shows that, regardless of the area studied: (1) the overburden is characterised by resistivities generally inferior to 50 Ωm; (2) the weathered and fractured horizons can be often mistaken for each other and have resistivities between 50 and 300 Ωm and 50 and 1,000 Ωm, respectively; and (3) the unweathered hard rock is quite distinct from the rest, with resistivities always superior to 1,000 Ωm. It is important to remember that the boundaries between the formations are unclear and carry some uncertainty. Such values are consistent with the ones proposed by Soro et al. (2017), Alle et al. (2018), Belle et al. (2019) and Nesny et al. (2019). The large data set used in this study allows one to statistically confirm and refine the resistivity ranges.

Here, resistivity was considered as principally impacted by weathering levels and clay content. Variations in

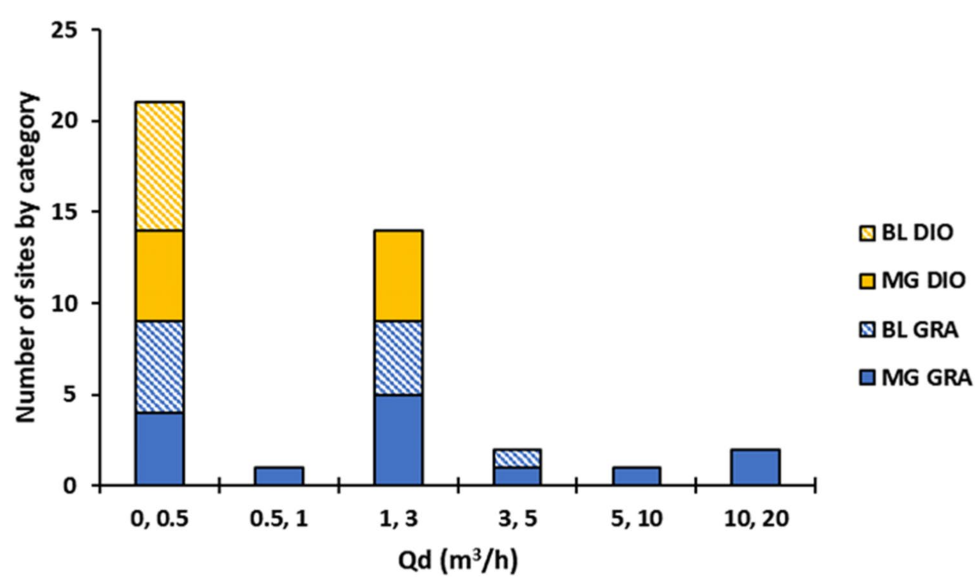

Fig. 7 Productivity by well lithology: granites and biotite granites (GRA group) and diorites, granodiorites and dolerites (DIO group). MG: Mongo watershed, BL: Barlo watershed

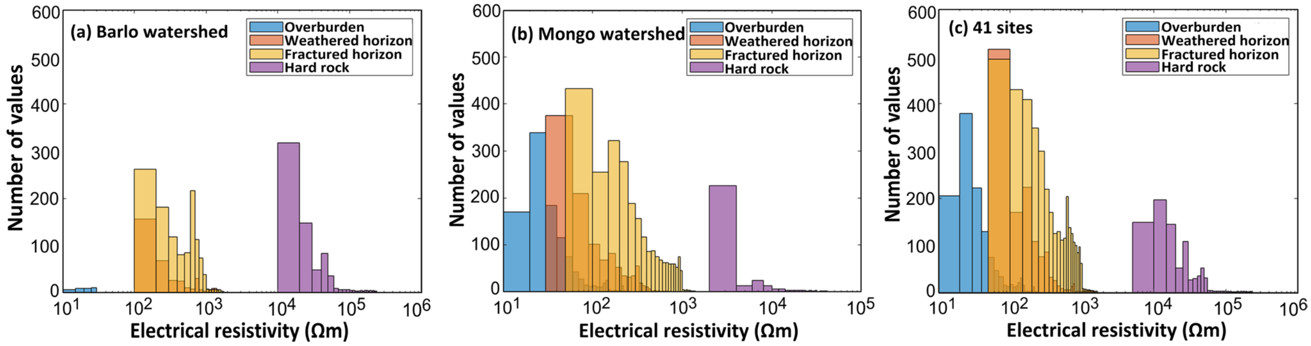

Fig. 8 Histograms of resistivity ranges by lithology for **a** Barlo watershed, **b** Mongo watershed, and **c** 41 sites

resistivity due to saturation levels might exist, but are deemed small, especially for depths larger than 5–10 m. For depths larger than that, it is likely geological formations do not become fully unsaturated, implying moderate variations in resistivity compared to those due to mineral composition and weathering levels. Noticeable variations in resistivity due to fluctuations in electrical conductivity of underground water, combined with porosity, are also unlikely. Measurements in different wells give an average water conductivity of ca. 300 μS/cm (33 Ωm) in weathered formations and ca. 500 μS/cm (20 Ωm) in deeper and fractured horizons (where there is less porosity).

A new classification based on geophysical characterisation

Based on the lithological data from the wells, the electrical profiles have been classified into four models, the statistics of which are presented in Fig. 9: (1) model A: composed of an overburden, well-developed weathered and fractured horizons, and unweathered rock, (2) model A*: similar to the previous model but with higher resistance on the surface in its first few metres, (3) model B: characterised by little or underdeveloped weathering throughout the profile or on the surface of the well, and (4) model C: marked by underdeveloped weathering and discontinuities.

For the structural models A, A* and B, there are positive (Qd ≥ 0.5 m^3/h) and negative (Qd ≈ 0 m^3/h) boreholes. Figure 9 illustrates examples of productive and non-productive wells for each of these three models as well as a negative case for Model C. Well names with the prefix MG are located in the Mongo watershed and those with BL in the Barlo watershed.

Model A: examples MG22 (Qd = 11 m^3/h) and MG23 (Qd ≈ 0 m^3/h) This model comprises four main layers: the overburden with a mean thickness of 10 m, the well-developed weathered and fractured horizons with mean thicknesses of 10 and 20 m respectively, and the unweathered hard rock at the base. The electrical resistivities of these layers increase progressively with depth. This pattern is found in 16 profiles, 12 of which have wells with high flow rates because there is little or no clay in the weathered horizon, while four profiles have wells with low flow rates in relation to clay formations in the overburden.

MG22 has (Fig. 9a): (1) low resistivity (30 Ωm) through the layer of clay and sand (11 m thick according to the well log); (2) a relatively low resistivity layer (40 Ωm) of alterites (23 m); (3) a moderate resistivity layer (130 Ωm) of fractured granite (18 m); and (4) a high resistivity layer (1,000 Ωm) of unweathered granite, not reached during drilling. This site is characterised by well-developed stratiform and fractured weathered horizons. The well installed at a distance of 120 m on the ERT setup, the assumed suitable FB point, was successful, with a flow rate of 11 m^3/h.

MG23 has (Fig. 9b): (1) a layer of fairly low resistivity (20 Ωm) sandy-clay formations (12 m thick according to the well log); (2) a moderately low resistivity layer (40 Ωm) of weathered granite (8 m); (3) a moderate resistivity layer (260 Ωm) of fractured granite (10 m); and (4) a high resistivity layer (3,000 Ωm) of unweathered granite. This site underperforms despite its well-developed weathering. Most likely, the presence of clay in the overburden prevents recharge of the underlying horizons. The well was placed here because of the initial electromagnetic profile data (EM34), in which clay formations may have been misinterpreted as fractures.

Model A*: examples MG15 (Qd = 12.7 m^3/h) and MG14 (Qd ≈ 0 m^3/h) This model is similar to model A but there is an additional thin resistant layer of sand, gravel or weathered granite on the surface. Productivity in this model is explained in the same way as in model A. Three sites with high flow rates (MG12, MG13 and MG15) and two non-productive sites (MG14 and MG09) represent this model.

Site MG15 has (Fig. 9c): (1) a thin, low-resistivity layer (30 Ωm) of clay (3 m); (2) a moderate resistivity layer (130 Ωm) of sand (14 m thick according to the well log); (3) a moderately low resistivity layer (50 Ωm) of weathered

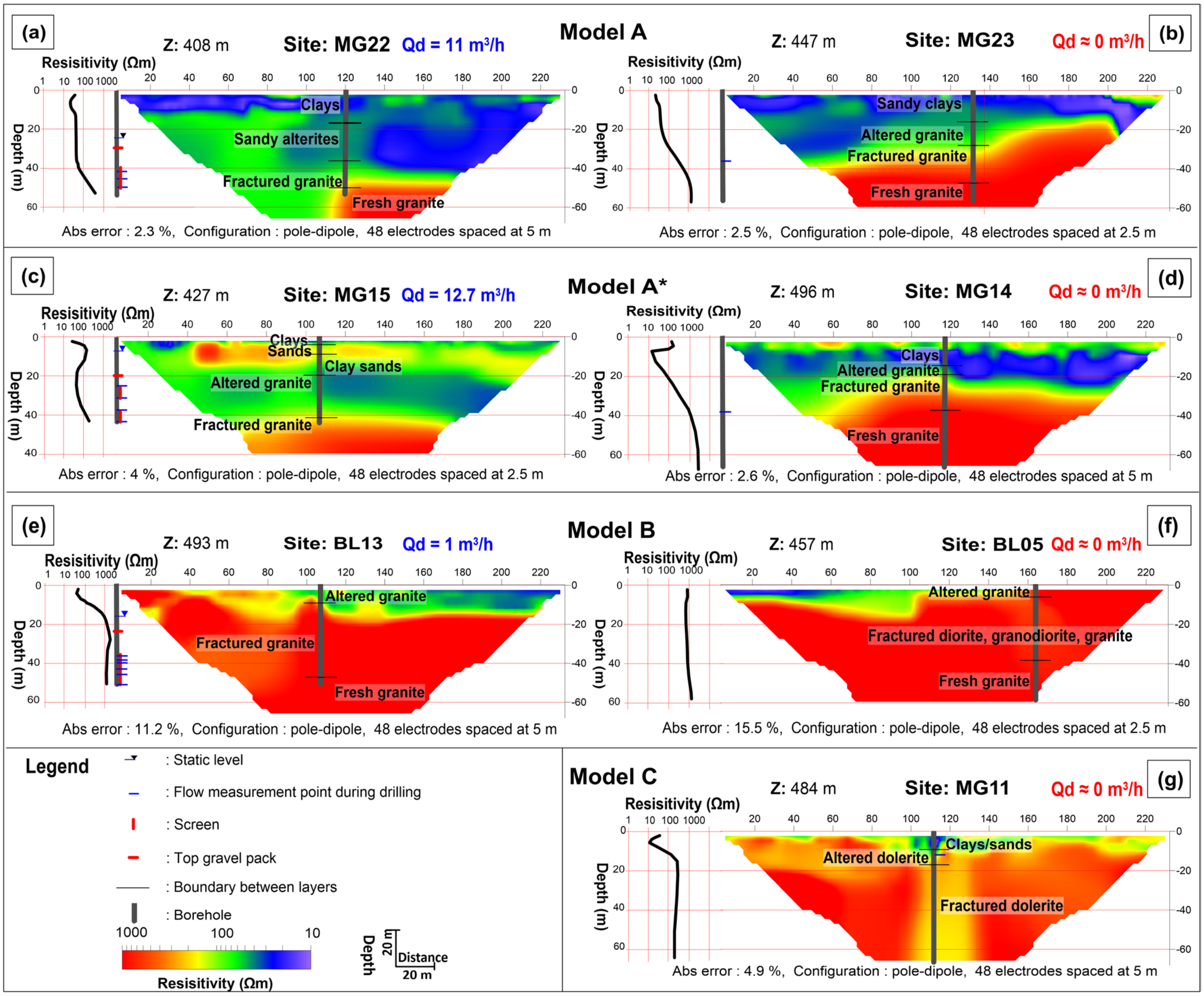

Fig. 9 Electrical resistivity tomography profiles for the four models: examples of productive (**a**, **c**, **e**) and non-productive (**b**, **d**, **f**, **g**) boreholes

granite (12 m); (4) a moderate resistivity layer (120 Ωm) of fractured granite (3 m); and (5) a high resistivity layer (1,000 Ωm) of undrilled, unweathered granite. This site shows that weathered and fractured horizons with little or no clay, but that are sufficiently thick (26 m of loose formations), lead to good flow rates even if overlaid by a resistant layer.

MG23 has (Fig. 9b): (1) a layer of fairly low resistivity (20 Ωm) sandy-clay formations (12 m thick according to the well log); (2) a moderately low resistivity layer (40 Ωm) of weathered granite (8 m); (3) a moderate resistivity layer (260 Ωm) of fractured granite (10 m); and (4) a high resistivity layer (3,000 Ωm) of unweathered granite. This site underperforms despite its well-developed weathering. Most likely, the presence of clay in the overburden prevents recharge of the underlying horizons. The well was placed here because of the initial electromagnetic profile data (EM34), in which clay formations may have been misinterpreted as fractures.

Model B: examples BL13 (Qd = 1.6 m^3 /h) and BL05 (Qd ≈ 0 m^3 /h) This model is characterised by an almost complete lack of overburden, an underdeveloped weathered horizon (average thickness less than 10 m), a fractured horizon about 20 m thick and unweathered rock. The electrical resistivities of this model evolve gradually with depth. Model B is observed in 18 site profiles, including five productive wells linked to a lateral water supply and 13 non-productive ones due to the absence of a storage reservoir.

BL13 has three main layers (Fig. 9e): (1) a weak topsoil layer (3 m according to the well log); (2) a moderate resistivity layer (250 Ωm) of weathered granite (15 m); (3) a moderate resistivity layer (950 Ωm) of fractured granite (30 m); and (4) a high resistivity layer (1,500 Ωm) of unweathered granite. The facies in this profile are laterally discontinuous. On one side, a weathered and fractured horizon (located on the last 120 m of the ERT survey) and on the other side, a fractured horizon in which the well is located (107.5 m on the ERT survey). This borehole has a very modest flow rate (Qd = 1 m^3/h), possibly due to the lateral recharge of the weathered and fractured horizons. The well could have encountered more productive formations had it been installed to the right of the ERT survey, ideally 160–220 m.

At BL05, the following layers succeed each other (Fig. 9f): (1) a weak layer of topsoil (1 m); (2) a moderate resistivity layer (750 Ωm) of weathered granite (7 m); (3) a moderate resistivity layer (750 Ωm) of diorite, granodiorite and fractured granite (44 m); and (4) a high resistivity layer (1,130 Ωm) of unweathered granite. This profile with little weathering is also marked by a lateral discontinuity, impeding the lateral feeding of the well.

Model C: example MG11 (Qd ≈ 0 m^3/h) This model resembles model B but is characterised by the presence of a discontinuity/fault. Site MG11 is unsuitable for a productive well due to the absence of a sufficiently developed weathered horizon to feed the fissures. In addition, discontinuities prevent any potential lateral recharge.

MG11 has (Fig. 9g): (1) a highly conductive layer (20 Ωm) of sandy clay (8 m); (2) a moderately conductive layer (130 Ωm) of weathered dolerite (8 m) and (3) a moderate resistivity layer (200 Ωm) of fractured dolerite. This profile stands out among the others because of its lateral and vertical discontinuity. It highlights a deepening corridor located perpendicular to the well between abscissas 100 and 120 m of the ERT survey. This zone could correspond to a fracture or a fault, not supplied with water because of no water reservoir in the overlying layers.

It is worth noting that among the sites described, wells MG22 and MG15 (models A and A*, 11 and 12.7 m^3/h respectively) are more productive than well BL13 (model B, 1 m^3/h). This difference is related to the thickness and to the degree of alteration of the weathered horizons in these different profiles.

From all the profiles, it appears that the most productive wells (Qd > 3 m^3/h) are characterised by a thick weathered layer or alterites (mean thickness of 12 m), containing little or no clay, and a thick fractured horizon (mean thickness of 20 m). Whereas the low flow rates wells (Qd ≈ 0 m^3/h) have little or no alterites, or have alterite layers dominated by clay.

Distribution of the different models

Two lithological sections (Fig. 10) reveal the geometry and continuity of the main aquifer strata. One is a longitudinal section (C1) along the main water drainage network of the Mongo watershed, oriented south–north (Fig. 10a), and the second represents a cross-section through the Barlo and Mongo watersheds, oriented WSW–ENE (Fig. 10b). These sections clearly show the different rocky formations in the region, even though the boreholes reveal varying thicknesses. In the longitudinal section (C1), the most productive wells, namely MG15 and MG13, have respective flow rates of 13 and 9 m^3/h, correspond to model A* and are located in the granite. They are characterised by little clay overburden, and well-developed weathered and fractured horizons (10–15 m and 13–18 m respectively) with significant water inflow in the upper part of the fractured horizon. Moderately productive wells, such as MG19 (2 m^3/h), MG05 (1.7 m^3/h) and MG24 (1.4 m^3/h), corresponds to model A and are also located in the granite. Nonproductive wells either have very little or no overburden or weathered layer, or clay is present in these formations. Cross-section (C2) is consistent with longitudinal section (C1). Cross-section also reveals reduced thicknesses for the overburden and weathered layer for nonproductive wells compared to productive ones.

The distribution of the different models and well productivity at the catchment scale were also analysed. The profiles and the associated models are presented on a topographic map produced through QGIS software, using 30-m resolution satellite images from the Shuttle Radar Topography Mission (SRTM; Fig. 11). The watersheds studied and the main drainage networks extracted from the DEM are shown. It should be noted that regardless of their Strahler order, the drainage networks are dry most of the year. The map also illustrates the lithology of the hard rock intersected by the wells and the development flow rate for each well.

Besides well productivity, the lithology seems to dictate the spatial distribution of the models. There are more A and A* models in wells located in granite, with a total of 14—11 A and 3 A* compared to only 7 in dolerite, diorite or granodiorite—5 A and 2 A*. As shown in the preceding (Fig. 7), wells located in granite are more productive than those in granodiorite: among the 11 model A wells in group GRA, 9 are positive and 0 negative, and the 3 A* wells have a Qd > 0.5 m^3/h. Conversely, among the five A wells in group DIO, three have a Qd above 0.5 m^3/h and two below, together with the two A* wells from group DIO.

Model B wells are observed in both groups (10 in group GRA and 9 in group DIO). Of the 10 model B wells in granite, 3 are productive and 7 nonproductive. Among the nine model B wells in dolerite, diorite or granodiorite, three are productive and six nonproductive. The lack of overburden and the underdeveloped weathered horizon in model B seem to be the key parameters influencing productivity, regardless of lithology. Model C closely resembles model B, but the wells are all nonproductive.

Model A and B wells are not evenly distributed in the two water catchment areas studied. Among the 16 A wells, 11 are in the Mongo Basin and five in the Barlo Basin; while the five A* wells are all located in the Mongo Basin. For Model B, 12 are in the Barlo catchment and seven in Mongo area. This difference could be related to the surface lithology: (1) dominance of granite versus granodiorite (unfortunately, these

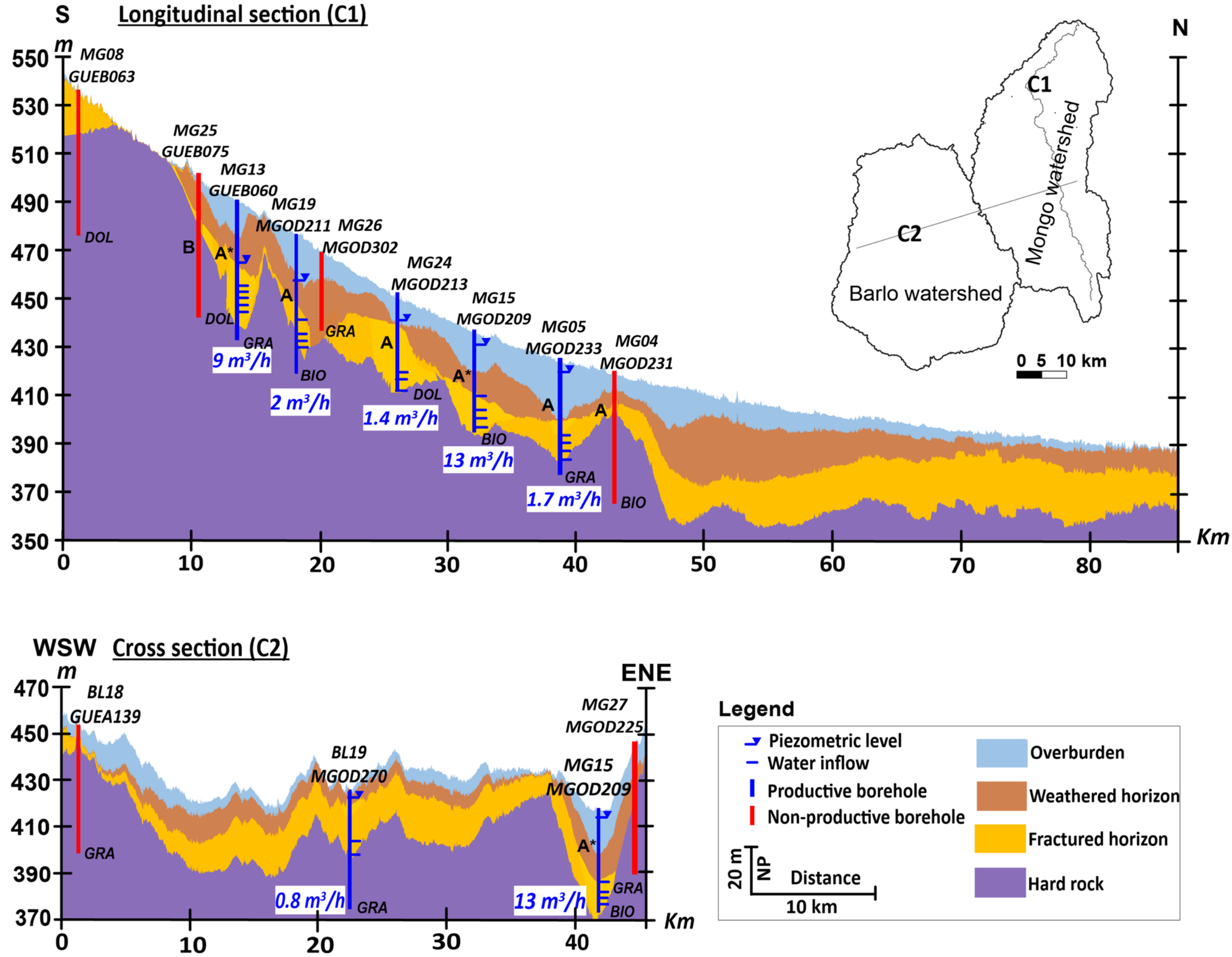

Fig. 10 **a** Longitudinal section of the Mongo watershed (C1) and **b** cross section of the Barlo and Mongo watersheds (C2). Lithology: BIO = Biotite, DOL = Dolerite, GRA = granite

formations cannot be distinguished through the geological map of the studied area) and (2) the presence of an overburden seems to be a key factor in the increase observed on the weathering processes of the hard rock below. Indeed, there is a lack of overburden in the Barlo catchment compared to Mongo. This study therefore highlights the role of the overburden, a horizon never before considered in such detail.

Combined approach: geological, geophysical and productivity data

Statistical analysis of the parameters according to the models

A statistical representation of the different variables is shown in Fig. 12, facilitating the comparison between the ranges of all parameters for the different models defined previously. The wells corresponding to model A are marked A^+ when they are high yield and A^- when they are low yield. It is clear from this analysis that some of the variables cannot be used in isolation to positively distinguish between high- and low-performing wells. This is the case, for example, for Z, TO, TWH, TFH, ρO and ρFH, which only partly explain well performance. For a site to be classed as suitable, it requires several complementary criteria; nonetheless, there are a few parameters, such as TAHR or T(O+WH), and ρWH (this last one needs to be relatively high, close to 100 Ωm, i.e., not too clayey, for the most productive sites A+ and A*+), that are statistically related to well productivity, suggesting they are key factors.

Normalised principal component analysis

Two different NPCAs were carried out (Fig. 13): a regional NPCA based on the combination of borehole productivity

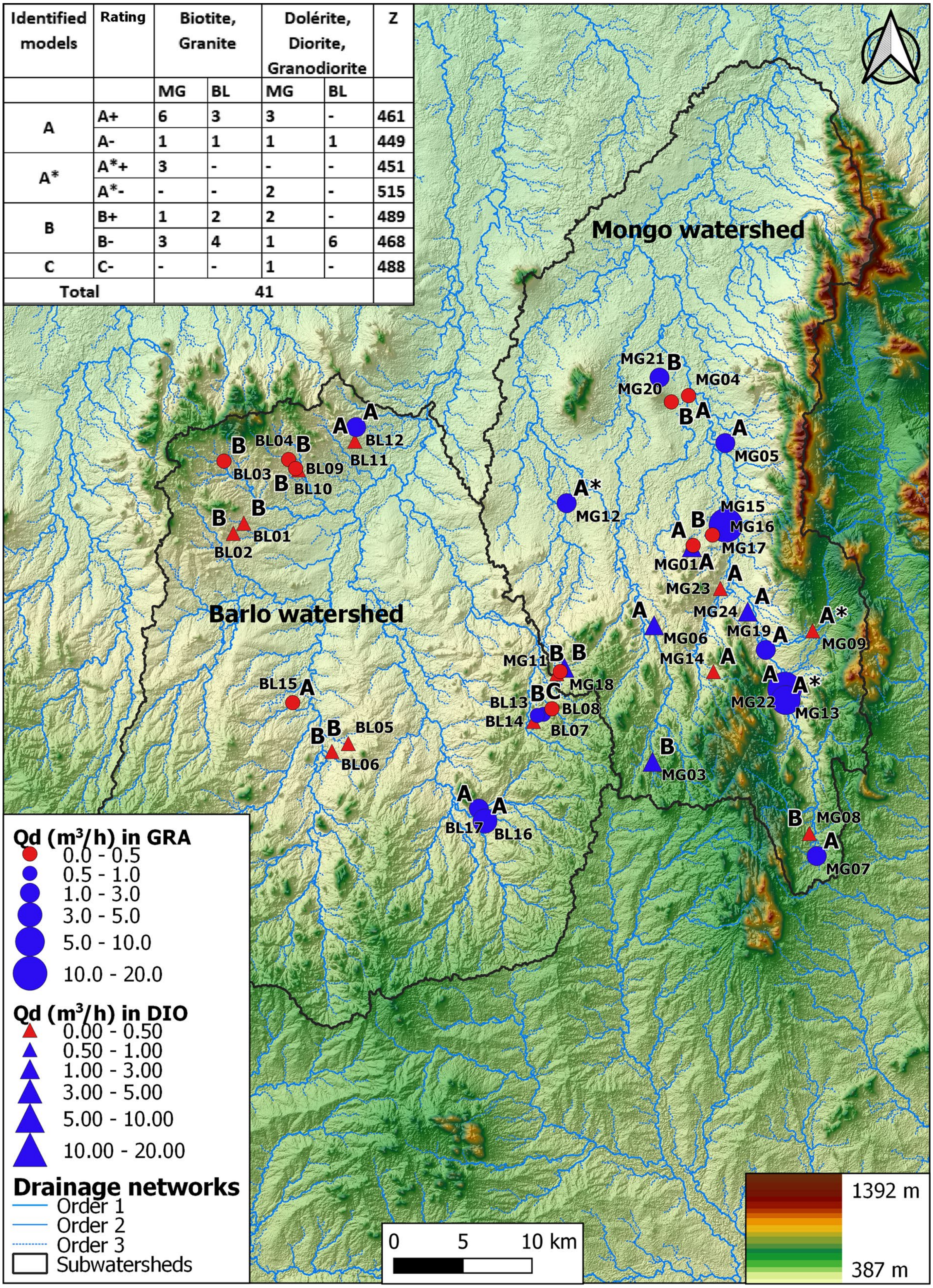

Identified models	Rating	Biotite, Granite		Dolérite, Diorite, Granodiorite		Z
		MG	BL	MG	BL	
A	A+	6	3	3	-	461
	A-	1	1	1	1	449
A*	A*+	3	-	-	-	451
	A*-	-	-	2	-	515
B	B+	1	2	2	-	489
	B-	3	4	1	6	468
C	C-	-	-	1	-	488
Total		41				

Fig. 11 Spatial distribution of the different models, local lithology and development flow rates on a geomorphological background. GRA: granites and biotite granites, DIO: diorites, granodiorites and dolerites

and geological parameters, and a NPCA at the scale of the two watersheds, including geophysical parameters.

Coupled analysis between geological criteria and production rate: regional scale (315 sites) Figure 13a,b illustrates the NPCAs applied to 315 and 41 sites respectively. Factors F1, F2 and F3 express 61.75% of the total variance of the data. The F1 axis expresses 26.86% of the variance and is determined by the grouping of variables corresponding to the well productivity (Qd – QFH). The variables Qd and QFH are strongly correlated ($R = 0.76$), reflecting the significant contribution of QFH to the total productivity of the wells (Qd). These variables are negatively correlated to the TD of the boreholes, explained by the fact that wells classed as low yield are often deeper than the others (Fig. 5a,b). In fact, drilling is pursued down to the basement until there is sufficient water inflow. The distribution of individual sites places the high-yield wells in the positive part of the F1 axis, on the side of productivity, and the low-yield wells in the negative part of this axis.

The F2 axis expresses 18.54% of the variance. Positive scores group TWH, Z and QWH, and T(O+WH) and TAHR. Thickness of the weathered horizon (TFH) scores negatively. This axis reveals the relationship between elevation Z with both thickness and flow rate of the weathered horizon (TWH and QWH), possibly explaining why the weathered horizon is preserved in the higher elevation areas, as opposed to its erosion in the valleys. There is also a strong correlation between T(O+WH) and TAHR, confirming the positive match between the data acquired when drilling the borehole and geological observations, and validating the descriptive quality of the latter.

Axis F3 expresses 16.35% of the variance and is defined by the opposition between the overburden thickness (TO and TCO) and the thickness of the weathered and fractured horizons [TWH, TFH and T(WH+FH)]. Site distribution places the wells of the Mongo watershed in the positive part of the F3 axis and the wells of Barlo in the negative part. The factorial plots F1–F2 and F1–F3 for 315 sites reveal that well productivity is largely dependent on the flow rate from the fractured horizon, independent of its thickness.

Coupled analysis between geological, geophysical and productivity criteria at the level of the two watersheds (41 sites) For the two watersheds (41 sites), factors F1, F2 and F3 express 70.28% of the total variance of the data (Fig. 13c,d). The F1 axis expresses 33.05% of the variance and is defined by the group "Qd–QFH–T(O+WH)–TAHR" representing well productivity on the positive side of the axis in opposition to TD and the resistivities of the weathered and fractured horizons (ρWH, ρFH). This means that the greater the flow rates, the lower the resistivity ranges of the weathered and fractured horizons (ρWH, ρFH; i.e., their resistivities move away from those of the unweathered bedrock) reflecting the advanced stage of weathering. This seems to contradict the fact that clay corresponds to the lowest electrical resistivities. It should be noted that the wells corresponding to models A and A*, characterised by a sufficiently thick weathered zone, are the most productive. These wells are mainly located in the Mongo watershed (76%), appearing on the positive side of the F1 axis. The correlation between (Qd–QFH) and weathered horizon thickness is also stronger among the 41 sites than for all 315 sites analysed together.

The F2 axis expresses 21.38% of the variance. The thickness of the overburden (TO and TCO) and the fractured horizon (TFH) appear opposite to the thickness and the flow rate of the weathered horizon (TWH and QWH) as well as to the elevation (Z) of the wells. As for the global analysis, this axis characterises the thickness of the formations and shows the influence of geomorphology (in this case the Z topography) on weathered formations thickness. It is clear that these loose formations are subject to the thickness of the overburden, and that this latter thickness is in opposition to the weathered horizon thickness.

The factor F3 expresses 15.85% of the variance. Positive scores define the flow rate in the weathered horizon (QWH), whereas negative scores describe the thickness of the weathered and fractured horizons [TWH and T(WH+FH)]. This shows that at the watershed level, TWH and QWH are not necessarily linked, contrary to what appears at the regional level (315 sites).

The analysis of these 41 sites shows that Qd is essentially controlled by the flow rate in the fractured horizon and by the thickness of the unconsolidated formations (mainly the overburden). The flow rate (Qd) seems to be independent of the flow rate of the weathered horizon and negatively correlated to the total depth (TD) and the resistivities (i.e., it is positively correlated to the conductivities) of the weathered and fractured horizons (ρWH and ρFH). A hypothesis to explain the latter two variables is that a high resistivity value is indicative of underdeveloped weathering in the fractured horizon (i.e., electrically resistant hard rock close to that of the unweathered layer), as opposed to a low resistivity value reflecting more advanced weathering.

Discussion

The current approach shows that the joint use of ERT, geology and well productivity is effective in improving the characterisation of aquifers and assisting in the construction of conceptual hydrogeological models.

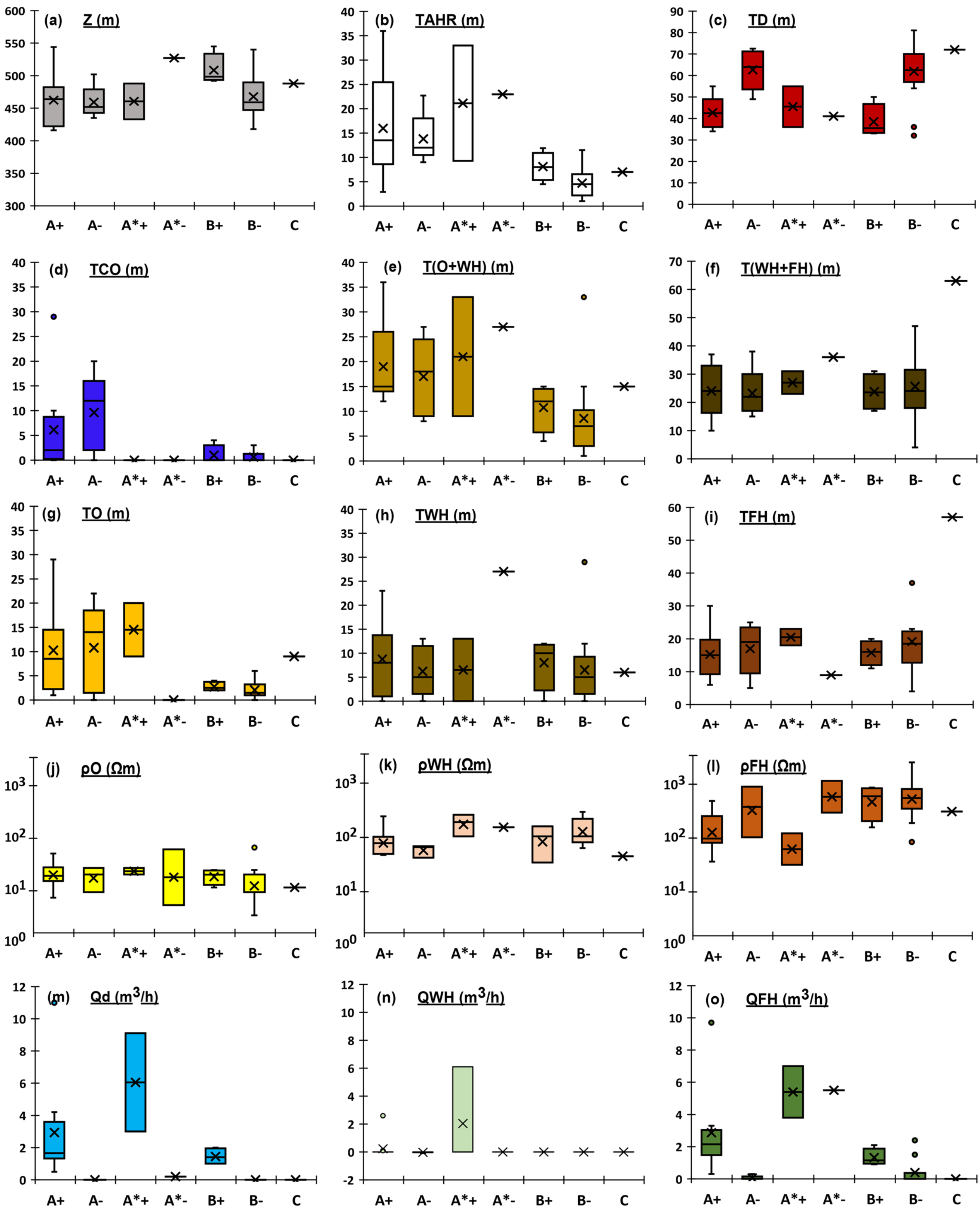

Fig. 12 **a–o** Boxplots of the main parameters selected for this study and their relationship to well productivity

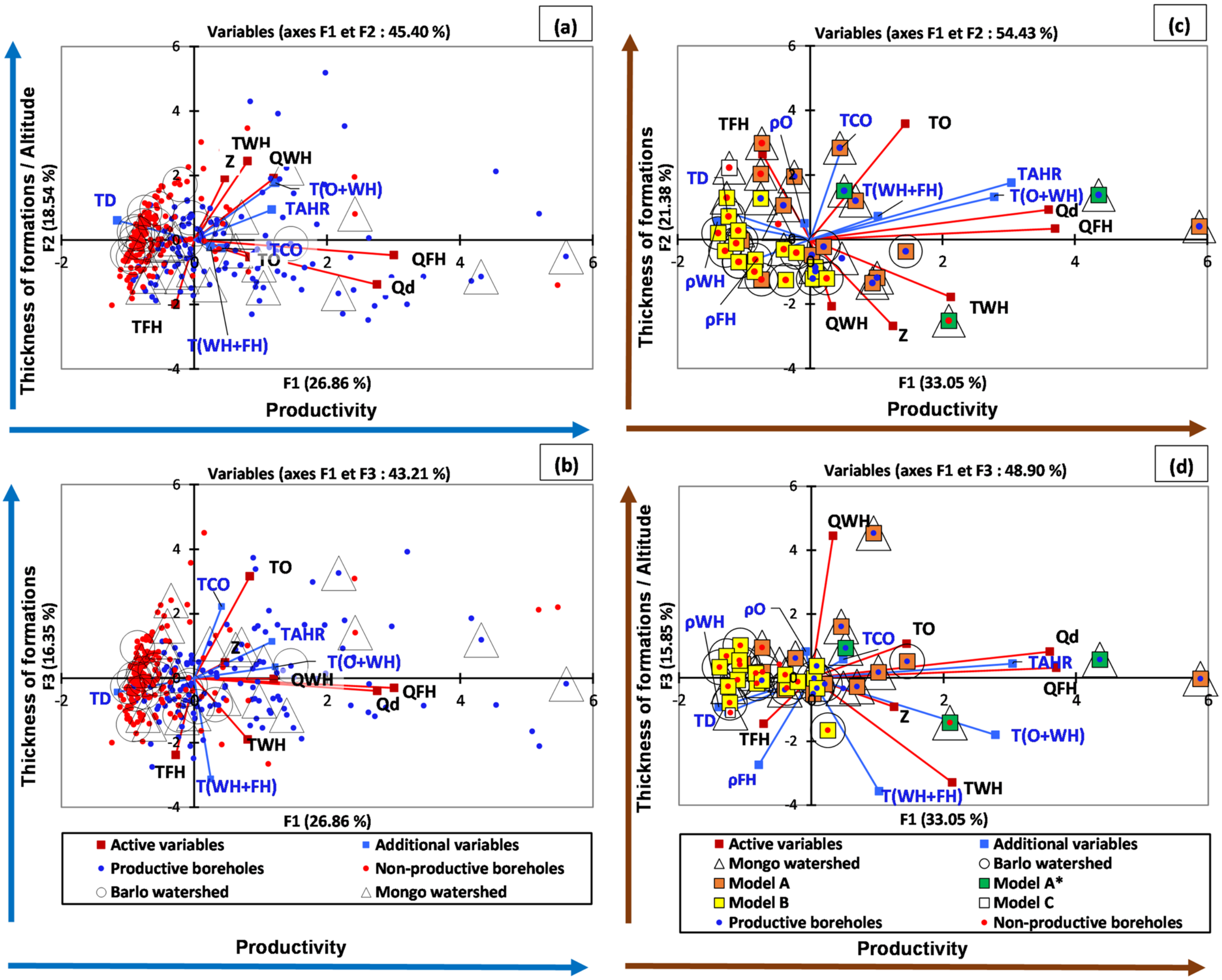

Fig. 13 NPCAs performed at the regional scale on 315 sites (**a**–**b**) and at the scale of the two experimental watersheds on 41 sites (**c**–**d**) on the parameters: Z, Qd, TO, TWH, QWH, TFH, QFH, TD, T(O+WH), TAHR, TCO, T(WH+FH), ρO, ρWH and ρFH

Contribution of electrical resistivity tomography to the detection of aquifers: comparison of the geoelectrical model with previous studies

ERT effectively differentiates the hydrogeological compartments of hard-rock aquifers. Albeit, the resistivity ranges for the weathered and fractured horizons can be continuous and thus these horizons can be difficult to distinguish using this parameter (Soro et al. 2017; Alle et al. 2018; Belle et al. 2019; Nesny et al. 2019). The large dataset in this study has helped better establish the probable facies based on electrical resistivity. The analysis of the geophysical profiles allowed four main formations to be clearly identified and their nature, thickness, arrangement, discontinuities and depth of water inflow to be specified where possible. These are, from top to bottom, the overburden, the layers with water-bearing potential (in particular, the weathered and fractured horizons), and the unweathered basement.

The overburden layer is well delineated with electrical resistivities below 50 Ωm, whereas the work of Soro et al. (2017), Alle et al. (2018), Belle et al. (2019) and Nesny et al. (2019) did not identify this layer. It includes laterite and bauxite layers and alluvium, and is composed of laterite with lateritic clay, compact clay with varying degrees of sand, clay, clayey sand and sand.

The weathered horizon resistivity ranges between 50 and 300 Ωm and is generally composed of two parts—an upper part made up of loose, moderately conductive formations and a lower part represented by consolidated, moderately resistant formations. The geoelectric properties of this horizon are comparable to results obtained in Benin (Nesny et al. 2019) and in Burkina-Faso (Soro et al. 2017).

The fractured horizon has highly variable electrical resistivities ranging from 50 to 1,000 Ωm. It is generally characterised by two series of fissures—sub-horizontal and sub-vertical—whose density decreases with depth. The geoelectric properties of this horizon are somewhat different to those proposed by Belle et al. (2019) at Saint-Galmier, France and at Sparouine, French Guyana, which can be explained by the fact that the areas studied did not undergo the same geological and climatic history.

The resistivity ranges for the weathered and the fractured horizon in the present study may be due to the presence or absence of water, the degree of weathering, and the mineralogical composition of the existing rocks, including biotite granites, diorites, granodiorites, dolerites, etc., as highlighted by Olona et al. (2010). These resistivity ranges do not allow for a precise identification of the boundary between these horizons.

The unweathered hard rock is clearly distinguishable from the other formations, with resistivities always above 1,000 Ωm. It is generally very resistant, except in certain specific places characterised by the presence of discontinuities: old fractures of tectonic origin, veins, dykes, etc. (Wyns et al. 2004; Maréchal et al. 2004). The geoelectric properties of the unweathered hard rock are comparable to those obtained in other regions, even when the geological and climatic contexts are different (Soro et al. 2017; Alle et al. 2018; Chandra and Tiwari 2022; Olivier et al. 2022; Ouedraogo et al. 2022).

Figure 14 illustrates these different layers as a conceptual diagram of the weathering profile. This conceptual model is consistent with that developed by Wyns et al. (2004), Dewandel et al. (2006), Lachassagne et al. (2011) and Belle et al. (2019), although the names and boundaries of the different sections are somewhat different.

Factors controlling well productivity

The statistical, spatial and multicriteria analyses carried out in this study have helped better assess and define the main factors controlling well productivity. Productivity is generally low, with a majority of wells studied exhibiting low flow rates. The highest flow rates (over 5 m^3/h) are observed in wells with a depth of 30–58 m. These results are similar to those of Abderamane et al. (2018) in the region, as well as those of Dibi et al. (2004), Maxime et al. (2014) and Odile et al. (2015) in the crystalline hard rock aquifers of Côte d'Ivoire. Data from previous programmes (PHPTC1/AFD 2008; PHPTC2/AFD 2013) have already established that maximum well depth should not exceed 80 m in the region. The aim is to avoid unnecessary but frequent overdrilling during well installation campaigns. Overdrilling does not improve well performance and impacts heavily on the budget allocated to projects. Several works carried out in West Africa have also defined optimal well depths in crystalline rock areas (Kouadio et al. 2010). In the Katiola region of Côte d'Ivoire, for example, the maximum drilling depths proposed are 80 m in granite and 100 m in shale (Maxime et al. 2014). In the far north region of Cameroon, the drilling depths not to be exceeded are 70 m for granitic formations, 55 m for metamorphic and 75 m for volcanic (Ewodo Mboudou et al. 2018). Spatial and multicriteria analyses, as well as geophysical profiles, show that well productivity is influenced

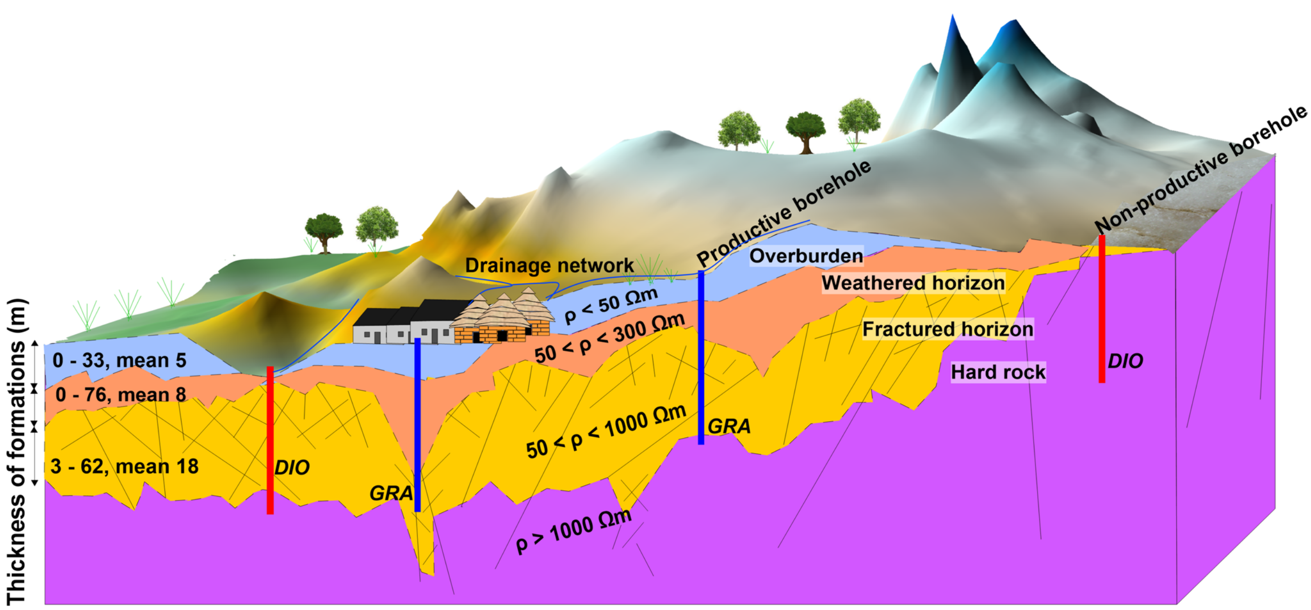

Fig. 14 Conceptual model of hard-rock aquifers as revealed by the present study

by the geometric, structural and geoelectrical properties of the subsurface, the lithological facies and geomorphology.

Geometry of the formations

Overburden is one of the key factors, but it plays a complex role due to its nature and thickness. Its role in well productivity is positive when it is permeable (alluvium, or of a low or no clay nature) and when its thickness does not exceed 20 m (see Fig. 6a). Sites where thicknesses exceed 20 m usually contain predominantly clay and are therefore impermeable. These results are consistent with those obtained in the Ouaddaï basement aquifers of eastern Chad (PREPAS 2018). Weathering processes appear to be enhanced by the presence of a minimum overburden thickness. The lower productivity in the Barlo catchment might be partially due to the limited extension (vertical and horizontal) of the overburden layer.

The weathered horizon also partly controls well productivity (see Figs. 6b, 9, 10, 13 and 14). The highest flow rates are found in the first 35 m of this horizon. Beyond that, flow rates decrease, a result that is in line with those of N'Go et al. (2005) and Maxime et al. (2014) for Côte d'Ivoire.

The cumulative thickness of the overburden and the weathered horizon, i.e., the thickness of the unconsolidated formations (TAHR), is significantly correlated with the flow rate as indicated in the 41-site NPCA (R = 0.7). Several authors have demonstrated that weathering is a key factor in well productivity (Wyns et al. 2004; Maréchal et al. 2004; Dewandel et al. 2006; Ahoussi et al. 2013; Vouillamoz et al. 2015; Worthington et al. 2016; Soro et al. 2017; Ewodo Mboudou et al. 2018; Alle et al. 2018; Belle et al. 2019; Lachassagne et al. 2021). Indeed, alterites and weathered formations, generally composed of sand and clay, have an important groundwater storage capacity, as confirmed by Legchenko et al. (2006) and Courtois et al. (2010).

The fractured horizon plays an essential role in well productivity, especially in the first 30 m. It ensures aquifer transmissivity provided it is beneath a weathered horizon and/or a suitable overburden ensuring the aquifer's storativity. Beyond 30 m, the water inflow and the flow rates decrease as a product of the lower fissure density in the rock as depth progresses. This has also been observed elsewhere (Dewandel et al. 2006, 2017; Chandra et al. 2008; Lachassagne et al. 2011, 2014, 2021; Ahoussi et al. 2013; Assemian et al. 2013).

Lithology of basement rocks

The main lithologies in the area studied are granites, biotite granites, diorites, granodiorites and dolerites (see Figs. 2 and 8). These rocks have different mineralogical compositions and hydrodynamic properties. Contrary to granites and biotite granites, the weathering of diorites, granodiorites and dolerites produces mainly clay (Isseini et al. 2013). The well logs confirm the presence of clay in zones dominated by weathered diorite, granodiorite and dolerite. This clay decreases the water infiltration capacity of such geologic formations (Rusagara et al. 2022).

Of the 20 high-yield wells, there are more of these wells in granitic areas (75%) than in areas with dolerite, diorite and granodiorite combined (25%; see Fig. 7). Similarly, the highest flow rates (>3 m^3/h) occur systematically in granitic areas. Low-yield wells are present in both areas: 57% for dolerites, diorites and granodiorites, 43% for granites. According to Wyns et al. (2015) and Lachassagne et al. (2021), biotite granites are extremely suitable for the development of a fractured horizon. Indeed, these micas have swelling properties that favour cracking.

Classification based on geophysics

A new classification is proposed, by synthesising the geometric and lithological information based on geophysics results. Models A and B appear to be dominant in the Guéra region and are perfectly coherent with the conceptual models presented by authors in the literature cited.

Models A and A* (the latter being somewhat resistant at the surface) are the most suitable for water productivity because they are characterised by well-developed weathered, stratified and fractured horizons. Of the 21 A and A* wells, most are classed as high yield (15 of 21 with Qd > 0.5 m^3/h). Of the 15 high-yield boreholes, 12 are in granite or biotite granite areas and only three are in dolerite, diorite and granodiorite areas.

Model B is the most unsuitable regardless of geological nature because it is characterised by little or no weathering, which allows for little or no groundwater storage. Of 19 wells (12 in Barlo and seven in Mongo), only 5 are high yield, including 3 in biotite granite areas. Model C characterises a single site located in a dolerite, nonproductive environment. It refers to poorly developed weathered and fractured horizons with lateral and vertical discontinuities.

The present research confirms the hypothesis that a thick weathered zone overlying a stratified fractured area constitutes a suitable hydrogeological target for the implantation of wells (Vouillamoz et al. 2015; Alle et al. 2018). It also reveals that the thickest weathered layers are generally clay-dominated (see Fig. 12d). It is therefore important to check the geological nature and particularly the proportion of clay in the overburden and the alterites, as this affects well productivity. As shown in the NPCAs, there is no correlation between well performance and one single parameter; several factors are required for a well to be productive.

Geomorphology

Geomorphology also seems to play a role in well productivity. The most productive wells are mainly located in low-lying areas near drainage networks (see Fig. 11). These low-lying areas seem to be conducive to the accumulation of surface water during the rainy season and actively contribute to the aquifer recharge. In riverine areas, there may also be a convergence of groundwater favourable to well productivity in these areas. Low-yield boreholes are preferentially located in the upstream areas of the watersheds. Areas of intense fracturing, such as fractured rock outcrops and drainage networks, may be the preferred areas for water infiltration (Millogo et al. 2020; Rusagara et al. 2022). The importance of geomorphology in identifying suitable areas has also been highlighted by Elbeih (2015) in Egypt, and Gómez-Escalonilla et al. (2022) in Mali.

Synthesis

To maximise the chances of drilling a productive well, it is preferable to choose a site with a lithology consisting essentially of granites and biotite granites, a type A or A* alteration model with well-developed weathered (linked to low resistivity values) and fractured horizons in the same location (average thickness around 10 and 20 m respectively), containing little or no clay. The presence of an alluvial or a low-clay overburden, with a thickness not exceeding 20 m, is a major asset. In addition to these criteria, some geomorphologies are better suited than others: downstream of the watershed, close to a watercourse or a drainage system.

The 41 sites are distributed as follows: 24 sites in the Mongo area, of which 15 have a well with a flow rate Qd > 0.5 m^3/h, and 17 sites in the Barlo area, of which five have a flow rate Qd > 0.5 m^3/h. In total, there are 20 high- and 21 low-yield wells. If the two watersheds are compared based on available well data, well productivity is better in the Mongo area than in the Barlo watershed. Indeed, Barlo does not have all of the previously cited criteria, with a very limited weathered layer (overburden and alterites). These unconsolidated formations may have suffered more significant erosion in the Barlo area, resulting in less productive wells than in the Mongo watershed.

Limitations

There are limitations to this hydrogeophysical approach to identifying suitable sites for the implantation of future hydraulic works. These can be due to the choice of the area studied by previous programmes. Indeed, as the hydraulic works were of a prospective nature, with a view to providing the population with drinking water, and not within a global framework of scientific research, the wells were drilled close to the villages (on an average distance of 3–4 km, to limit travel in order to obtain drinking water), which leads to a sampling bias. More representative sampling, according to different contexts, could further improve the knowledge of this complex crystalline environment. It is worth noting that the present study is focused on the Guéra massif. Similar analysis should be carried out in other granitic basement areas in other countries to confirm the conclusions made in section 'Synthesis'.

From a lithological point of view, there are also small inconsistencies in terms of the quality of the geological descriptions provided at the time of drilling. The work was carried out by different technicians, each of whom describes according to his or her design/training on an observational basis—for example, it is very difficult to distinguish the base of the alterites from the roof of the fractured horizon from the lithological descriptions.

It is also important to note that the well's geophysical probabilistic analysis was only vertical, without considering its surroundings. Finally, the boundaries between the different formations identified are not clear-cut and present uncertainties.

Principal component analysis is a descriptive statistics method that allows for a simplified representation of a large dataset by reducing the number of factors. In the present PCA, all boreholes—productive or nonproductive—were taken into account, which means that the flow rates are not well distributed, with 56% zero flow rates and only a few high flow rates, rendering difficult the analysis of the results. It is, however, a very useful method for understanding a large dataset, making it possible to highlight statistical links between borehole productivity and "explanatory" parameters such as lithology, depth, clay content, etc.

Conclusion

In the crystalline basement of Guéra region, the exploitation of groundwater is the only alternative to meet the drinking water needs of the population and ensure the development of socio-economic activities. Electrical resistivity tomography, with geological, hydrogeological and geomorphological analyses, has enabled a better understanding of the geometry and characteristics of the main hydrogeological targets for new or future drilling. Future analysis of ERT sections based on the results of this study could help increase the probability of drilling positive wells. Areas where the estimated thicknesses from ERT of the overburden (maximum of 20 m) and weathered horizons (on the order of 10–20 m) are not optimal should be avoided. The conceptual hydrogeological models produced here are consistent with recent models of hard-rock aquifers proposed in the literature. The geoelectrical properties of these models were compared with other profiles from the literature cited. Discrepancies were observed and can be attributed to different geological contexts and histories, and possibly even to different climates.

This analysis of aquifer system productivity in Guéra reveals relatively modest flow rates (with a mean of 1 m^3/h). The probability of having productive boreholes and high flow rates seems to be higher in granites and biotite granites. The most productive structures are characterised by well-developed weathered and fractured horizons, a lithology with little or no clay, and a geomorphology suitable for water infiltration and recharge. The water inlets are located between 30 and 60 m deep, under an overburden and alterites. The alterites provide significant groundwater storage, but most of the resource is contained in the upper part of the fractured horizon, the first 30 m below the base of the alterites; therefore, the fractured horizon ensures water transmissivity.

This hydro-geophysical approach contributes to a better understanding of the hydrogeological properties of the Guéra hard-rock aquifer and demonstrates that ERT combined with geological and hydrogeological data is an effective means of understanding the subsoil, and of building a conceptual hydrogeological model. It constitutes a decision-support tool for the identification of suitable layers for the construction of water points in order to improve access rates to drinking water for the population, applicable on a national and international scale. It is therefore desirable that during future well installation campaigns in hard-rock aquifers, the actors concerned appropriate the current methodology to avoid hazardous installations and their economic and social consequences.

Acknowledgements The authors would like to express their sincere thanks to these organisations for the grants awarded and thank Antea Group and the Chad Ministry for Water for providing them with the well database.

Funding This work was supported by the Service de Coopération et d'Action Culturelle (SCAC) of the French Embassy in Chad and by the International Atomic Energy Agency (IAEA) in the framework of the RAF7019 project

Declarations

Conflicts of Interest On behalf of all authors, the corresponding author states that there is no conflict of interest.

References

9th FED (2011) Accès à l'eau potable et assainissement [Access to drinking water and sanitation)]. FED/2005/017076 et FED/2006/018625. Etudes hydro-géophysiques d'implantation de 450 forages dans le Guéra et le Batha. Rapport final Egis Bceom International/ANTEA/CIAT. République du Tchad, Ministère de l'Eau, 35 pp

10th FED (2016) Plan d'investissement en matière d'accès à l'eau potable et à l'assainissement dans le Guéra [Investment plan for access to drinking water and sanitation in Guéra]. Rapport de synthèse d'investissement, SUEZ Consulting, Ministry of Water, N'Djamena, Chad, 115 pp

Abderamane H, Massing O, Adoum I, Yaya I (2018) Contribution of remote sensing and geophysics to hydrogeological reconnaissance in the basement areas of the Guéra region: case of the city of Mongo (Chad). International Journal of Engineering Sciences and Research Technology 7:241–257. https://doi.org/10.5281/ZENODO.1173456

Ahoussi KE, Koffi YB, Kouassi AM, Soro G, Soro N, Biemi J (2013) Fonctionnement hydrodynamique des aquifères discontinus de la région d'Abidjan-Agboville (Sud de la Côte d'Ivoire) [Hydrodynamic functioning of discontinuous aquifers in the Abidjan-Agboville Region (South of Ivory Coast)]. International Journal of Geography and Geology 2:52–69. https://doi.org/10.18488/journal.10/2013.2.5/10.5.52.69

Alle IC, Descloitres M, Vouillamoz J-M, Yalo N, Lawson FM, Adihou AC (2018) Why 1D electrical resistivity techniques can result in inaccurate siting of boreholes in hard rock aquifers and why electrical resistivity tomography must be preferred: the example of Benin, West Africa. J Afri Earth Sci 139:341–353. https://doi.org/10.1016/j.jafrearsci.2017.12.007

Assemian EA, Kouame FK, Djagoua ÉV, Affian K, Jourda JPR, Adja M, Lasm T, Biemi J (2013) Étude de l'impact des variabilités climatiques sur les ressources hydriques d'un milieu tropical humide : Cas du département de Bongouanou (Est de la Côte d'ivoire) [Study of the impact of climate variability on water resources in a humid tropical environment: Case of the Bongouanou department (East of Ivory Coast)]. Rev Sci Eau 26:247–261. https://doi.org/10.7202/1018789ar

Belle P, Lachassagne P, Mathieu F, Barbet C, Brisset N, Gourry J-C (2019) Characterization and location of the laminated layer within hard rock weathering profiles from electrical resistivity tomography: implications for water well siting. Geol Soc London Spec Pub 479:187–205. https://doi.org/10.1144/SP479.7

Bouchot V, Kaboré EB, Itard Y, Courtois N, Somé S, Sy AT, Récoché G (2011) Burkina Faso, géoressource et société: un projet scientifique Sud-Nord au service d'une gestion raisonnée des géoressources en Afrique intertropicale [Burkina Faso, geo-resources and society: a south–north scientific project serving the rational management of geo-resources in intertropical Africa]. Vertigo. https://doi.org/10.4000/vertigo.10435

Briški M, Stroj A, Kosović I, Borović S (2020) Characterization of aquifers in metamorphic rocks by combined use of electrical resistivity tomography and monitoring of spring hydrodynamics. Geosciences 10:137. https://doi.org/10.3390/geosciences10040137

Chandra S, Tiwari VM (2022) Rapid 3D geophysical imaging of aquifers in diverse hydrogeological settings. Water Secur 15:100111. https://doi.org/10.1016/j.wasec.2022.100111

Chandra S, Ahmed S, Ram A, Dewandel B (2008) Estimation of hard rock aquifers hydraulic conductivity from geoelectrical measurements: a theoretical development with field application. J Hydrol 357:218–227. https://doi.org/10.1016/j.jhydrol.2008.05.023

Courtois N, Lachassagne P, Wyns R, Blanchin R, Bougaïré FD, Somé S, Tapsoba A (2010) Large-scale mapping of hard-rock aquifer properties applied to Burkina Faso. Ground Water 48:269-283. https://doi.org/10.1111/j.1745-6584.2009.00620.x

Dewandel B, Lachassagne P, Wyns R, Maréchal J-C, Krishnamurthy NC (2006) A generalized 3-D geological and hydrogeological conceptual model of granite aquifers controlled by single or multiphase weathering. J Hydrol 330:260–284. https://doi.org/10.1016/j.jhydrol.2006.03.026

Dewandel B, Lachassagne P, Zaidi FK, Chandra S (2011) A conceptual hydrodynamic model of a geological discontinuity in hard rock aquifers: example of a quartz reef in granitic terrain in South India. J Hydrol 405:474–487. https://doi.org/10.1016/j.jhydrol.2011.05.050

Dewandel B, Caballero Y, Perrin J, Boisson A, Dazin F, Ferrant S, Chandra S, Maréchal J-C (2017) A methodology for regionalizing 3-D effective porosity at watershed scale in crystalline aquifers. Hydrol Process 31:2277–2295. https://doi.org/10.1002/hyp.11187

Dibi B, Inza D, Goula BTA, Savane I, Biemi J (2004) Analyse statistique des paramètres influençant la productivité des forages d'eau en milieu cristallin et cristallophyllien dans la région d'Aboisso (sud-est de la côte d'Ivoire) [Statistical analysis of parameters influencing water drilling productivity in crystalline and crystallophyllian environments in the Aboisso region (southeast of Ivory Coast)]. https://api.semanticscholar.org/CorpusID:140182971. Accessed January 2024

Dinard M, Abderamane H, Mahamat Nour A (2021) Contribution of remote sensing and geophysics to optimize the location of boreholes in the basement zone: the case of the city of Abéché (CHAD). GSC Advanced Research and Reviews 8:146–159. https://doi.org/10.30574/gscarr.2021.8.3.0201

Elbeih SF (2015) An overview of integrated remote sensing and GIS for groundwater mapping in Egypt. Ain Shams Eng J 6:1–15. https://doi.org/10.1016/j.asej.2014.08.008

Ewodo Mboudou G, Bon AF, Bineli E, Ntep F, Ombolo A (2018) Caractérisation de la productivité des aquifères du socle de la région de l'extrême Nord, Cameroun [Characterization of the productivity of the basement aquifers in the Far North region, Cameroon]. J Cameroon Acad Sci 14:25. https://doi.org/10.4314/jcas.v14i1.3

Foppen JW, Lutterodt G, Rau GC, Minkah O (2020) Groundwater flow system analysis in the regolith of Dodowa on the Accra Plains, Ghana. J Hydrol: Region Stud 28:100663. https://doi.org/10.1016/j.ejrh.2020.100663

Gaye CB, Tindimugaya C (2019) Review: Challenges and opportunities for sustainable groundwater management in Africa. Hydrogeol J 27:1099–1110. https://doi.org/10.1007/s10040-018-1892-1

Gómez-Escalonilla V, Marie-Louise V, Elisa D, Moussa I, Giaime O, Daira D, Pedro M-S, Francesco H (2021) Delineation of groundwater potential zones by means of ensemble tree supervised classification methods in the Eastern Lake Chad basin. Geocarto International, pp 1–28. https://doi.org/10.1080/10106049.2021.2007298

Gómez-Escalonilla V, Martínez-Santos P, Martín-Loeches M (2022) Preprocessing approaches in machine-learning-based groundwater potential mapping: an application to the Koulikoro and Bamako regions, Mali. Hydrol Earth Syst Sci 26:221–243. https://doi.org/10.5194/hess-26-221-2022

Howard G, Bartram J, Pedley S, Schmoll O, Chorus I, Berger P (2006) Groundwater and public health: managing the quality of drinking-water sources. IWA, London

INSEED (2009) Deuxième Recensement Général de la Population et de l'Habitat. Résultats globaux définitifs [Second General Census of Population and Housing: final global results]. Ministère des Finances, de l'Economie et du Plan, N'Djamena, Chad, 60 pp

IPCC (2014) Climate Change 2014: synthesis report. Contribution of Working Groups I, II and III to the Fifth Assessment Report of the Intergovernmental Panel on Climate Change]. IPCC, Geneva, Switzerland, 151 pp

Isseini M, Hamit A, Abderamane M (2013) The tectonic and geologic framework of the Mongo area, a segment of the Pan-African Guera Massif in Central Chad: evidences from field observations and remote sensing. Revue Scientifique du Tchad, pp 16

Kamagaté B, Séguis L, Favreau G, Seidel J-L, Descloitres M, Affaton P (2007) Processus et bilan des flux hydriques d'un bassin versant de milieu tropical de socle au Bénin (Donga, haut Ouémé) [Processes and water flow balance of a watershed in a tropical basement environment in Benin (Donga, upper Ouémé)]. C R Geosci 339:418–429. https://doi.org/10.1016/j.crte.2007.04.003

Kouadio EK, Nagnin S, Savane I (2010) Stratégie d'optimisation de la profondeur des forages en contexte de socle: application à la région du Denguélé, Nord-Ouest de la Côte d'Ivoire [Drilling depth optimization strategy in a basement context: application to the Denguélé Region, northwest of Ivory Coast]. Rev Sci Eau 23:1–15. https://doi.org/10.7202/038921ar

Kouamé KF, Lasm T, De Dreuzy JR, Akaffou AG, Bour O, Davy P (2010) Contribution d'un modèle hydrogéologique à fractures discrètes à l'étude des aquifères fracturés du socle Archéen de Touba (Nord-Ouest, Côte d'Ivoire) [Contribution of a discrete fracture hydrogeological model to the study of fractured aquifers in the Archean basement of Touba (North-West, Ivory Coast)]. Rev Sci Eau 23:41–56. https://doi.org/10.7202/038924ar

Koudou A, Adiaffi B, Sombo AP, Amani EME, Biemi J (2013) Concept of a decision-making tool for the groundwater prospecting in hard rock area: southeast of Ivory Coast. Geo-Eco-Trop 37:211–226

Kusnir I (1995) Géologie, ressources minérales et ressources en eau du Tchad [Geology, mineral resources and water resources of Chad]. Travaux et documents scientifiques du Tchad. Connaissance du Tchad, Ministère du plan et de la coopération, N'Djamena, Chad, 115 pp

Lachassagne P, Wyns R, Bérard P, Bruel T, Chéry L, Coutand T, Desprats J-F, Strat P (2001) Exploitation of high-yields in hard-rock aquifers: downscaling methodology combining GIS and multicriteria analysis to delineate field prospecting zone. Ground Water 39:568–581. https://doi.org/10.1111/j.1745-6584.2001.tb02345.x

Lachassagne P, Wyns R, Dewandel B (2011) The fracture permeability of Hard Rock Aquifers is due neither to tectonics, nor to unloading, but to weathering processes: weathering and permeability of hard rock aquifers. Terra Nova 23:145–161. https://doi.org/10.1111/j.1365-3121.2011.00998.x

Lachassagne P, Aunay B, Frissant N, Guilbert M, Malard A (2014) High-resolution conceptual hydrogeological model of complex basaltic volcanic islands: a Mayotte, Comoros, case study. Terra Nova 26:307–321. https://doi.org/10.1111/ter.12102

Lachassagne P, Dewandel B, Wyns R (2021) Review: Hydrogeology of weathered crystalline/hard-rock aquifers—guidelines for the operational survey and management of their groundwater resources. Hydrogeol J 29:2561–2594. https://doi.org/10.1007/s10040-021-02339-7

Leborgne R, Rivett MO, Wanangwa GJ, Sentenac P, Kalin RM (2021) True 2-D resistivity imaging from vertical electrical soundings to support more sustainable rural water supply borehole siting in Malawi. Appl Sci 11:1162. https://doi.org/10.3390/app11031162

Legchenko A, Descloitres M, Bost A, Ruiz L, Reddy M, Girard J-F, Sekhar M, Mohan Kumar MS, Braun J-C (2006) Resolution of MRS applied to the characterization of hard rock aquifers. Ground Water 44:547–554. https://doi.org/10.1111/j.1745-6584.2006.00198.x

Lemaitre-Basset T, Oudin L, Thirel G (2022) Evapotranspiration in hydrological models under rising CO2: a jump into the unknown. Clim Change 172:36. https://doi.org/10.1007/s10584-022-03384-1

Leridon H (2015) Afrique subsaharienne: une transition démographique explosive [Sub-Saharan Africa: an explosive demographic transition]. Revue Futuribles 407:5–21

Loke MH, Barker RD (1996) Rapid least-squares inversion of apparent resistivity pseudosections by a quasi-Newton method. Geophys Prospect 44:131–152. https://doi.org/10.1111/j.1365-2478.1996.tb00142.x

Loke MH, Acworth I, Dahlin T (2003) A comparison of smooth and blocky inversion methods in 2D electrical imaging surveys. Explor Geophys 34:6

MacDonald AM, Bonsor H, Dochartaigh BÉÓ, Taylor RG (2012) Quantitative maps of groundwater resources in Africa. Environ Res Lett 7:024009. https://doi.org/10.1088/1748-9326/7/2/024009

Maréchal JC, Dewandel B, Subrahmanyam K (2004) Use of hydraulic tests at different scales to characterize fracture network properties in the weathered-fractured layer of a hard rock aquifer: fracture network properties in hard rock. Water Resour Res 40:W1508. https://doi.org/10.1029/2004WR003137

Matheron G (1966) Présentation des variables régionalisées [Presentation of regionalized variables]. J Société Fr Stat 107:263–275 http://www.numdam.org/article/JSFS_1966__107__263_0.pdf

Maurice L, Taylor RG, Tindimugaya C, MacDonald AM, Johnson P, Kaponda A, Owor M, Sanga H, Bonsor CH, Darling WG, Gooddy D (2019) Characteristics of high-intensity groundwater abstractions from weathered crystalline bedrock aquifers in East Africa. Hydrogeol J 27:459–474. https://doi.org/10.1007/s10040-018-1836-9

Maurya VP, Chandra S, Sonkamble S, Lohithkumar K, Nagaiah E, Selles A (2021) Electrically inferred subsurface fractures in the crystalline hard rocks of an experimental hydrogeological park, Southern India. Geophysics 86:WB9–WB18. https://doi.org/10.1190/geo2020-0327.1

Maxime GF, Solange OYM, Théophile G, Théolphile L, Jean B, Nestor KYK (2014) Analyse de la productivité des aquifères de fissures du socle paléoprotérozoïque de la région de Katiola (Centre-Nord de la Côte d'Ivoire) [Analysis of the productivity of fractured aquifers in the Paleoproterozoic basement of the Katiola region (Central-North of Ivory Coast)]. Eur Sci J 10:79–98

Millogo C, Bakouan C, Sawadogo S (2020) Caractérisation physicochimique des eaux de surface et des altérites du bassin versant du lac Bam, Centre Nord du Burkina Faso [Physicochemical characterization of surface waters and laterites in the Lake Bam watershed, North-Central Burkina Faso]. Afri Sci 17:137–150

N'Go Y, Goné D, Savané I, Goblé M (2005) Potentialités en eaux souterraines des aquifères fissurés de la région d'Agboville (Sud-Ouest de la Côte d'Ivoire): caractérisation hydroclimatique et physique [Groundwater potential of fractured aquifers in the Agboville region (Southwest of Ivory Coast): hydroclimatic and physical characterization]. Afrique Science : Revue Internationale des Sciences et Technologie 1:127–144. https://doi.org/10.4314/afsci.v1i1.35401

Nesny AY, Nicaise Y, Bertrand AH, Marc YT, George A (2019) Apport de la télédétection et de la géophysique dans la cartographie des fractures hydrauliquement actives en zone de socle au Centre-Ouest du Benin [Contribution of remote sensing and geophysics to the mapping of hydraulically active fractures in the basement area of Central-West Benin]. Eur Sci J 15:27. https://doi.org/10.19044/esj.2019.v15n27p426

Odile BL, Ake ST, Etienne G, Ahoussi KE, Oga MS, Biemi J, Akossi D (2015) Productivité des forages d'eau en milieu cristallin et cristallophyllien dans la région de Daoukro (Centre-Est de la Côte d'Ivoire) [Productivity of water drilling in crystalline and crystallophyllian environments in the Daoukro region (Central-East of Ivory Coast)]. Synthèse : Revue des Sciences et de la Technologie 30:76–90. https://doi.org/10.12816/0027945

Olivier KKJ, Jules MOM, Parfait SA, Frédéric P, Brou D, Didier G (2022) Elaboration of a hydrogeological conceptual model by application of electrical resistivity tomography: case of the Lobo catchment (Centre-Western Côte d'Ivoire). Sci Afri 16:e01234. https://doi.org/10.1016/j.sciaf.2022.e01234

Olona J, Pulgar JA, Fernández-Viejo G, López-Fernández C, González-Cortina JM (2010) Weathering variations in a granitic massif and related geotechnical properties through seismic and electrical resistivity methods. Near Surf Geophys 8:585–599. https://doi.org/10.3997/1873-0604.2010043

Ouedraogo M, Pessel M, Durand V, González-Cortina A, Kamagate B, Savane I (2022) Multifrequency electromagnetic method for the hydrogeophysical characterization of hard-rock aquifers: the case of the upstream watershed of White Bandama (northern Ivory Coast). BSGF Earth Sci Bull 193:11. https://doi.org/10.1051/bsgf/2022009

Oursingbé M, Zhonghua T, Oyelola BW, Mahamadou Z (2012) Groundwater exploration in the basement of Lake-Iro District-Chad, using electrical resistivity imaging approach. Int J Phys Sci 7:2721–2729. https://doi.org/10.5897/IJPS11.961

PHPTC1/AFD (2008) Réalisation de 73 forages de reconnaissance dans le Guera (66) et le Batha (07) [Completion of 73 exploratory drillings in Guera (66) and Batha (07)]. Final report no. A 50701, Document ANTEA/IRAM, Annexe Hydro 2, Ministry of Water, N'Djamena, Chad, 22 pp

PHPTC2/AFD (2013) Réalisation de 138 forages de reconnaissance dans le Guera (120) et le Batha (18) [Completion of 138 exploratory drillings in Guera (120) and Batha (18)]. RFinal report no. A R 83860, Document ANTEA/IRAM, Annexe Hydro 2, Ministry of Water, N'Djamena, Chad, 58 pp

PREPAS (2018) Programme de Renforcement de l'Elévage Pastoral dans les régions du Batha, de l'Ennedi et du Wadi-Fira au Tchad. Etude hydrogéophysique [Livestock Strengthening Program in the Batha, Ennedi, and Wadi-Fira regions of Chad: hydrogeophysical study]. Rapport de synthèse de la prospection géophysique (Etape 3), Unité de Coordination Technique et Fiduciaire du PREPAS, ANTEA-AGRITCHAD, Chad, 341 pp

Ruelle P, Ben Salah D, Vauclin M (1986) Méthodologie d'analyse de la variabilité spatiale d'une parcelle agronomique: application à l'échantillonnage [Methodology for analyzing the spatial variability of an agronomic plot: application to sampling]. Agronomie 6:529–539. https://doi.org/10.1051/agro:19860605

Rusagara R, Koïta M, Plagnes V, Jost A (2022) Groundwater recharge pathways to a weathered-rock aquifer system in a dryland catchment in Burkina Faso. Hydro J 30:1489–1512. https://doi.org/10.1007/s10040-022-02506-4

Sagna P, Ndiaye O, Diop C, Niang AD, Sambou PC (2015) Les variations récentes du climat constatées au Sénégal sont-elles en phase avec les descriptions données par les scénarios du GIEC [Are recent climate variations observed in Senegal in conformity with the descriptions given by the IPCC scenarios]? Pollution Atmosphérique : Climat, Santé, Société 17. https://inondations-dakar.org/dataset/les-variations-recentes-du-climat-constatees-au-senegal. Accessed Jan 2024

Sander P (2007) Lineaments in groundwater exploration: a review of applications and limitations. Hydrogeol J 15:71–74. https://doi.org/10.1007/s10040-006-0138-9

Schneider J-L (1989) Géologie et hydrogéologie de la République du Tchad (PhD) [Geology and Hydrogeology of the Republic of Chad]. https://www.worldcat.org/title/geologie-et-hydrogeologie-de-la-republique-du-tchad/oclc/490171090. Accessed January 2024

Schneider J-L (2001) Géologie, Archéologie et Hydrogéologie [Geology, archaeology, and hydrogeology]. Préface de mémoire 1, Ministère de l'Environnement et de l'Eau, N'Djamena, Chad, 462 pp

Schneider J-L, Wolf JP (1992) Carte géologique et cartes hydrogéologiques à 1/1 500 000 de la republique du Tchad [Geological map and hydrogeological maps at 1/1,500,000 of the Republic of Chad]. Mémoire explicatif, Document BRGM no. 209, vols 1 and 2, BRGM, Orléans, France, 531 pp

Soro DD, Koïta M, Biaou CA, Outoumbe E, Vouillamoz J-M, Yacouba H, Guérin R (2017) Geophysical demonstration of the absence of correlation between lineaments and hydrogeologically usefull fractures: case study of the Sanon hard rock aquifer (central northern Burkina Faso). J Afri Earth Sci 129:842–852. https://doi.org/10.1016/j.jafrearsci.2017.02.025

Taylor R, Howard K (2000) A tectono-geomorphic model of the hydrogeology of deeply weathered crystalline rock: evidence from Uganda. Hydrogeol J 8:279–294

Taylor RG, Todd MC, Kongola L, Maurice L, Nahozya E, Sanga H, MacDonald AM (2013) Evidence of the dependence of groundwater resources on extreme rainfall in East Africa. Nat Climate Change 3:374–378. https://doi.org/10.1038/nclimate1731

Valdes D (2005) Variabilité spatiale du fonctionnement hydrologique de l'aquifère karstique de la craie (Département de l'Eure, France) [Spatial variability of the hydrological functioning of the chalk karst aquifer (Eure Department, France)]. Université de Rouen, Mont-Saint-Aignan, France, 288 pp

Vouillamoz J-M, Lawson FMA, Yalo N, Descloitres M (2014) The use of magnetic resonance sounding for quantifying specific yield and transmissivity in hard rock aquifers: the example of Benin. J Appl Geophys 107:16–24. https://doi.org/10.1016/j.jappgeo.2014.05.012

Vouillamoz J-M, Lawson FMA, Yalo N, Descloitres M (2015) Groundwater in hard rocks of Benin: regional storage and buffer capacity in the face of change. J Hydrol 520:379–386. https://doi.org/10.1016/j.jhydrol.2014.11.024

Worthington SRH, Davies GJ, Alexander EC (2016) Enhancement of bedrock permeability by weathering. Earth-Sci Rev 160:188–202. https://doi.org/10.1016/j.earscirev.2016.07.002

Wyns R (2020) Les altérations supergènes et la géodynamique de la lithosphère [Supergene alterations and the geodynamics of the lithosphere]. Bull Inf géol Bass 57:60–66

Wyns R, Baltassat J-M, Lachassagne P, Legchenko A, Vairon J, Mathieu F (2004) Application of proton magnetic resonance soundings to groundwater reserve mapping in weathered basement rocks (Brittany, France). Bull Soc Géol France 175:21–34. https://doi.org/10.2113/175.1.21

Wyns R, Dewandel B, Lachassagne P (2015) Origin of fracturation in hard-rock aquifers: what are the factors that control the properties of the fissured horizon? Extended abstract at Vingtièmes journées techniques du Comité Français d'Hydrogéologie de l'Association Internationale des Hydrogéologues: Aquifères de socle: le point sur les concepts et les applications opérationnelles La Roche-sur-Yon, France, June 2015. https://doi.org/10.13140/RG.2.1.3699.3124